98-03

ELSEVIER

Physica D 116 (1998) 191–224

PHYSICA D

A Boussinesq system for two-way propagation of nonlinear dispersive waves

Jerry L. Bona [a,*], Min Chen [b]

[a] *Department of Mathematics and the Texas Institute for Computational and Applied Mathematics, The University of Texas, Austin, TX 78712, USA*

[b] *Department of Mathematics, The Pennsylvania State University, University Park, PA 16802, USA*

Received 30 August 1996; received in revised form 28 July 1997; accepted 15 October 1997
Communicated by R. Temam

Abstract

In this report, we study the system

$$N_t + W_x + (NW)_x - \tfrac{1}{6}N_{xxt} = 0, \qquad W_t + N_x + WW_x - \tfrac{1}{6}W_{xxt} = 0, \tag{*}$$

which describes approximately the two-dimensional propagation of surface waves in a uniform horizontal channel of length L_0 filled with an irrotational, incompressible, inviscid fluid which in its undisturbed state has depth h. The non-dimensional variables $N(x,t)$ and $W(x,t)$ represent the deviation of the water surface from its undisturbed position and the horizontal velocity at water level $\sqrt{2/3}h$, respectively. The natural initial-boundary-value problem corresponding to the situation wherein the channel is fitted with a wavemaker at both ends is formulated and analyzed theoretically. We then present a numerical algorithm for the approximation of solutions of the system (*) and prove the algorithm is fourth-order accurate both in time and in space, is unconditionally stable, and has optimal computational complexity, which is to say the operation cost per time step is of order M where M is the number of grid points in the spatial discretization. Further, we implement the algorithm as a computer code and use it to study head-on collisions of solitary waves. Our numerical simulations are compared with existing theoretical, numerical and experimental results. We have tentatively concluded that the system (*) is a good candidate for modeling two-dimensional surface water waves. Copyright © 1998 Elsevier Science B.V.

Keywords: Boussinesq systems; Solitary waves; Two-way propagation of water waves

1. Introduction

Consideration is given to the propagation of waves in a uniform horizontal channel of length L_0 filled to a depth h with an incompressible perfect fluid. Assuming that the wave motion is generated irrotationally and that it is uniform across the width of the channel, the two-dimensional Euler equations are the full equations of motion. Even

* Corresponding author.

PII S0167-2789(97)00249-2

the two-dimensional version of the Euler equations are currently challenging both theoretically and with respect to the numerical approximation of solutions. Consequently, when the practical need arises to model waves, further approximations are often made. Assuming that the maximum deviation a of the free surface from its undisturbed position is small relative to h (small-amplitude waves), that the typical wavelength λ is large relative to h (long waves), and that the Stokes number $S = a\lambda^2/h^3$ is of order 1, the Euler equations may be formally approximated by a restricted, four-parameter class of model equations derived by Bona et al. [6], having the form

$$\eta_t + u_x + (u\eta)_x + au_{xxx} - b\eta_{xxt} = 0, \qquad u_t + \eta_x + uu_x + c\eta_{xxx} - du_{xxt} = 0, \tag{1}$$

in scaled variables, where a, b, c and d are real constants satisfying the restrictions

$$\begin{aligned} a &= \tfrac{1}{2}(\theta^2 - \tfrac{1}{3})\lambda, \qquad b = \tfrac{1}{2}(\theta^2 - \tfrac{1}{3})(1 - \lambda), \\ c &= \tfrac{1}{2}(1 - \theta^2)u, \qquad d = \tfrac{1}{2}(1 - \theta^2)(1 - \mu), \end{aligned} \tag{2}$$

where $0 \le \theta \le 1$, and $\lambda, \mu \in \mathbb{R}$. Subscripts connote partial differentiation, the independent variable x corresponds to distance along the channel while t is proportional to elapsed time. The dependent variable $\eta = \eta(x, t)$ is proportional to the derivation of the liquid's free surface from its rest position at the location x at time t and $u = u(x, t)$ is proportional to the horizontal velocity at the height θh.

As pointed out in [6], all the models in (1) yield approximations which, like the classical Boussinesq system ([8], $a = b = c = 0$, $d = \frac{1}{3}$), are formally accurate to order $\epsilon = a/h$. An interesting issue immediately presents itself as to which of these models should be chosen in concrete modeling situations. The theory developed by Craig [15] is not helpful in this instance because it deals with an ill-posed model, though his theory is definitive for unidirectional, Korteweg–de Vries-type models. The developments in [6] indicate that many of the possibilities in (1) are mathematically ill posed or that they do not preserve energy or other physical quantities conserved by the full Euler equations. After these are eliminated, there still remain several potentially useful classes of models of the form depicted in (1).

It is our purpose to examine in some detail one of the more promising of the potentially useful models derived in [6], namely

$$\begin{aligned} &\eta_t - \tfrac{1}{6}h^2\eta_{xxt} = -hw_x - (\eta w)_x, \qquad w_t - \tfrac{1}{6}h^2 w_{xxt} = -g\eta_x - ww_x, \\ &\quad \text{for } (x, t) \in \Omega = [0, L_0] \times [0, T_0]. \end{aligned} \tag{3}$$

The system (3) is (1) with $a = c = 0$, $b = d = \frac{1}{6}$, but written in physical variables, where x is the distance along the channel, t the elapsed time, g the acceleration of gravity, h the undisturbed depth, and η is such that $h + \eta(x, t)$ is the total depth at location x at time t, as before. The dependent variable $w = w(x, t)$ is the horizontal velocity at the water level $\sqrt{2/3}h$ at the location x along the channel at time t. To simplify the notation in the rest of the paper, we will resort to the standard non-dimensional variables (already in use in the systems in (1)), $\hat{x} = x/h$, $\hat{t} = t/\sqrt{h/g}$, $N = \eta/h$, and $W = w/c_0$, where $c_0 = \sqrt{gh}$. The corresponding scaled Boussinesq system is

$$\begin{aligned} &N_{\hat{t}} - \tfrac{1}{6}N_{\hat{x}\hat{x}\hat{t}} = -W_{\hat{x}} - (NW)_{\hat{x}}, \qquad W_{\hat{t}} - \tfrac{1}{6}W_{\hat{x}\hat{x}\hat{t}} = -N_{\hat{x}} - WW_{\hat{x}}, \\ &\quad \text{for } (\hat{x}, \hat{t}) \in \Omega = [0, L] \times [0, T], \end{aligned} \tag{4}$$

where $L = L_0/h$ and $T = T_0/\sqrt{h/g}$.

The theory developed in [6] for certain of the systems in (1) was for the pure initial-value problems posed on the entire real line, and thus pertains to wave motion far from the ends of a channel or for very long-crested waves in field situations. In this report, attention will be directed to the initial- and boundary-value problem for which there is specified

$$\begin{aligned} N(0,\hat{t}) &= h_1(\hat{t}), & N(L,\hat{t}) &= h_2(\hat{t}), \\ W(0,\hat{t}) &= v_1(\hat{t}), & W(L,\hat{t}) &= v_2(\hat{t}), \\ N(\hat{x},0) &= f_1(\hat{x}), & W(\hat{x},0) &= f_2(\hat{x}). \end{aligned} \tag{5}$$

The consistency requirements for the initial- and boundary-conditions are the obvious ones dictated by continuity considerations, namely

$$h_1(0) = f_1(0), \quad h_2(0) = f_1(L), \qquad v_1(0) = f_2(0), \quad v_2(0) = f_2(L). \tag{6}$$

The problem (4)–(6) is appropriate to the situation where, in addition to disturbances already in the channel initially, wave motion can be added at both ends of the channel. Our particular interest in this problem stems from some forthcoming water-tank experiments in which wave motion is initiated by wavemakers at both ends of the channel. One reason for choosing the system (4) from the various well-posed possibilities in (1) is that it is reasonably straightforward to implement the initial-boundary-value problem in (5) for the system (4). Another salient point is that accurate and efficient numerical algorithms are readily developed for the system (4).

The plan of the paper is as follows. In Section 2, the initial-boundary-value problem (4) and (5) is written as a system of integral equations. Existence, uniqueness, and regularity results for the solutions of (4)–(6) are established by recourse to the integral equations. A numerical algorithm having optimal order of efficiency for the approximation of solutions of (4)–(6) is then proposed in Section 3. The scheme is based on the system of integral equations. In Section 4, it is shown that the numerical scheme is unconditionally stable and fourth-order convergent in both space and time. The algorithm is then implemented as a computer code and the rate of convergence tested in Section 5. Numerical simulations of the head-on collision of solitary waves are also presented in this section. The paper concludes with a brief summary.

2. Theoretical results

In this section, we prove that corresponding to given compatible initial- and boundary-data as in (5) and (6), there exists a unique solution to (4) and (5), defined at least on $[0, L] \times [0, T]$ for some $T > 0$, and we examine the regularity of this solution. The existence of a solution is established by converting (4) and (5) into integral equations and applying the contraction-mapping principle. The regularity then follows from the fact that solutions of the integral equations are exactly as smooth as the data affords. The argument is similar to that proposed in [2,3] for a single equation which models unidirectional waves and in [7] for the pure initial-value problem for another Boussinesq-type system (see also [6]). In what follows, we drop the carets adorning the independent variables in (4).

To begin, write the system (4) in the form

$$(1 - a^{-2}\partial_x^2)N_t = -W_x - (NW)_x, \qquad (1 - a^{-2}\partial_x^2)W_t = -N_x - WW_x,$$

where $a^2 = 6$. Inverting the operator $1 - a^{-2}\partial_x^2$ subject to the boundary conditions in (5), one obtains

$$N_t(x,t) = \int_0^L G(x,s)(-W_s - (NW)_s)\,\mathrm{d}s + S(L-x)h_1' + S(x)h_2',$$

$$W_t(x,t) = \int_0^L G(x,s)(-N_s - WW_s)\,\mathrm{d}s + S(L-x)v_1' + S(x)v_2',$$

where

$$G(x,s) = -\frac{a[\cosh(a(L-x-s)) - \cosh(a(L-|x-s|))]}{2\sinh(aL)}$$

and

$$S(x) = \frac{\sinh(ax)}{\sinh(aL)}.$$

Since $G(x,s)$ is continuous with respect to s, continuously differentiable except at $s = x$, and $G(x,L) = G(x,0) = 0$ for all $x \in [0,L]$, the integrals on the right-hand sides may be integrated by parts, thereby leading to

$$\begin{aligned} N_t &= \int_0^L K(x,s)(W+NW)\,\mathrm{d}s + S(L-x)h_1' + S(x)h_2' \equiv \mathcal{F}_1(x,t,N,W), \\ W_t &= \int_0^L K(x,s)(N+\tfrac{1}{2}W^2)\,\mathrm{d}s + S(L-x)v_1' + S(x)v_2' \equiv \mathcal{F}_2(x,t,N,W), \end{aligned} \tag{7}$$

with

$$K(x,s) = \frac{\partial G}{\partial s} = \frac{a^2}{2}(S(L-x-s) + \operatorname{sign}(x-s)S(L-|x-s|)).$$

Now integrating the equations in (7) with respect to the temporal variable, one obtains

$$\begin{aligned} N(x,t) &= f_1(x) + \int_0^t \int_0^L K(x,s)(W+NW)\,\mathrm{d}s\,\mathrm{d}r \\ &\quad + S(L-x)(h_1(t)-h_1(0)) + S(x)(h_2(t)-h_2(0)), \\ W(x,t) &= f_2(x) + \int_0^t \int_0^L K(x,s)(N+\tfrac{1}{2}WW)\,\mathrm{d}s\,\mathrm{d}r \\ &\quad + S(L-x)(v_1(t)-v_1(0)) + S(x)(v_2(t)-v_2(0)). \end{aligned} \tag{8}$$

Note that any classical solution of (4) and (5) satisfies the integral equations in (8) since all the steps followed in the derivation of (8) may then be justified.

Denote by $C^k(a,b)$ the Banach space of k-times continuously differentiable functions defined on $[a,b]$, equipped with the norm

$$\|f\|_{C^k} = \sup_{0\le j\le k} \sup_{a\le x\le b} |f^{(j)}(x)|.$$

We will systematically abbreviate $\|f\|_{C^0}$ by $\|f\|$.

Before presenting the local existence and uniqueness result, it is convenient to prove some properties of the mapping $\mathcal{M}$ defined by

$$\mathcal{M}(v)(x) = \int_0^L K(x,s)v(s)\,\mathrm{d}s \tag{9}$$

for any $v \in C(0,L)$.

Lemma 1. There is a constant c_1 depending only on L and constants D_k, $k = 0, 1, \ldots$, depending on k and L such that

(a) if $A_j = \sup_{0\le x\le L}\{\int_0^x |K_x^{(j)}(x,s)|\,ds + \int_x^L |K_x^{(j)}(x,s)|\,ds\}$, $j \ge 0$, then

$$A_j \le (\sqrt{6})^j c_1,$$

and

(b) if $v \in C^k(0, L)$ for some $k \ge 0$, then $\mathcal{M}(v) \in C^{k+1}(0, L)$ and

$$\|\mathcal{M}(v)\|_{C^{k+1}} \le D_k \|v\|_{C^k}.$$

In (a), $K_x^{(j)}$ connotes the jth partial derivative of K with respect to x, computed classically on the intervals $[0, x]$ and $[x, L]$.

Proof. Observing that for $|x| \le L$, $|S(x)| \le 1$ and that $K(x, s)$ is continuous in s except at $s = x$, where there is a jump discontinuity with

$$K(x, x^+) - K(x, x^-) = a^2 = 6, \tag{10}$$

one easily obtains that $|K(x, s)| \le 2a^2$ which yields that A_0 is bounded by the constant $2a^2L$. Since for $|x| \le L$, $|S'(x)|$ is bounded by a constant depending only on L, and K_x' is continuous, it is seen that A_1 is bounded by a constant which also depends only on L. It is easy to verify that for $x \ne s$,

$$K_x^{(m+2)}(x, s) = a^2 K_x^{(m)}(x, s) \quad \text{for any } m \ge 0, \tag{11}$$

which yields (a) for $j \ge 0$ with c_1 being any constant which bounds A_0 and A_1.

Let $v \in C(0, L)$ and denote $\mathcal{M}(v)$ by ϕ. Using part (a), one sees that

$$\|\phi\| \le \sup_{0\le x\le L} \int_0^L |K(x, s)|\,ds \|v\| \le c_1 \|v\|.$$

Using (10) and (11), one shows that

$$\phi'(x) = \int_0^L K_x'(x, s)v(s)\,ds + 6v(x),$$

and that

$$\phi^{(m+2)}(x) = 6\phi^{(m)}(x) + 6v^{(m+1)}(x) \quad \text{for } m \ge 0.$$

The first equation yields $\phi \in C^1$ in the case $v \in C^0$ with

$$\|\phi(x)\|_{C^1} \le (c_1 + 6)\|v\|,$$

and the second equation, when used as the basis for an inductive argument, yields (b) for any $k \ge 0$. □

For any Banach space X (for instance $X = C^k$), the space $C(0, T; X)$ is the Banach space of continuous maps $u : [0, T] \to X$ with the norm

$$\|u\|_{C(0,T;X)} = \sup_{0\le t\le T} \|u(t)\|_X.$$

The product space $X \times X$ will be abbreviated by X^2; it carries the norm

$$\|\mathbf{f}\|_X = \max\{\|f_1\|_X, \|f_2\|_X\}$$

for $\mathbf{f} = (f_1, f_2)$.

We are now ready to prove the local existence and global uniqueness of solutions of the system of integral equations (8) corresponding to specified auxiliary data as in (5).

Theorem 2. Let $\mathbf{f} = (f_1, f_2) \in C(0, L)^2$, $\mathbf{h} = (h_1, h_2)$, $\mathbf{v} = (v_1, v_2) \in C(0, T)^2$ for some $T, L > 0$. Suppose $\mathbf{f}$, $\mathbf{h}$ and $\mathbf{v}$ to satisfy the compatibility conditions (6). Define $\|\mathbf{f}\| = \max\{\|f_1\|_{C(0,L)}, \|f_2\|_{C(0,L)}\}$, $\|\mathbf{h}\| = \max\{\|h_1\|_{C(0,T)}, \|h_2\|_{C(0,T)}\}$, and $\|\mathbf{v}\| = \max\{\|v_1\|_{C(0,T)}, \|v_2\|_{C(0,T)}\}$. Then there is a $T_0 = T_0(T, L, \|\mathbf{f}\|, \|\mathbf{h}\|, \|\mathbf{v}\|) \le T$ and a unique solution pair (N, W) in $C(0, T_0; C(0, L))^2$ that satisfies (8). Moreover, for any $T_1 \le T$, there is at most one solution of (8) in $C(0, T_1; C(0, L))^2$.

Proof. Let $\mathcal{C} = C(0, T_0; C(0, L))^2$ and write the pair of integral equations in (8) in the tidy form

$$\mathbf{U} = A\mathbf{U},$$

where $\mathbf{U} \equiv (N, W)$. It will be shown that the operator A defined by the right-hand side of (8) has a fixed point in $\mathcal{C}$ for suitably chosen T_0 by using the contraction-mapping theorem. From Lemma 1 and the compatibility conditions, it is readily adduced that if $\mathbf{U} \in \mathcal{C}$, then $A\mathbf{U} \in \mathcal{C}$. Suppose now that both $\mathbf{U}$ and $\mathbf{W}$ lie in the closed ball B_R of radius R about $\mathbf{0}$ in $\mathcal{C}$; then we have the helpful inequality

$$\begin{aligned}\|A\mathbf{W}(x,t) - A\mathbf{U}(x,t)\|_{\mathcal{C}} &\le c_1(1 + \|\mathbf{U}\|_{\mathcal{C}} + \|\mathbf{W}\|_{\mathcal{C}}) \int_0^{T_0} \|\mathbf{U} - \mathbf{W}\|_{\mathcal{C}}\, d\tau \\ &\le c_1 T_0(1 + 2R)\|\mathbf{U} - \mathbf{W}\|_{\mathcal{C}} \\ &\equiv \Theta\|\mathbf{U} - \mathbf{W}\|_{\mathcal{C}}. \end{aligned} \tag{12}$$

If $\Theta < 1$, then A is a contraction-mapping. For $\mathbf{U} \in B_R$, let B denote the terms in (8) involving the initial- and boundary-values, namely

$$B = \begin{pmatrix} f_1(x) + S(L - x)(h_1(t) - h_1(0)) + S(x)(h_2(t) - h_2(0)) \\ f_2(x) + S(L - x)(v_1(t) - v_1(0)) + S(x)(v_2(t) - v_2(0)) \end{pmatrix}.$$

It is obvious that $\|B\|_{C(0,T;C(0,L))^2} \le b \equiv \|\mathbf{f}\| + 2(\|\mathbf{h}\| + \|\mathbf{v}\|)$, and therefore

$$\|A\mathbf{U}\|_{\mathcal{C}} = \|A\mathbf{U} - A\mathbf{0} + B\|_{\mathcal{C}} \le \Theta\|\mathbf{U}\|_{\mathcal{C}} + \|B\|_{\mathcal{C}} \le \Theta R + b.$$

Thus if we choose $R = 2b$ and $T_0 = T_0(b) = 1/2(1 + R)c_1$, it is seen that

$$\Theta = \tfrac{1}{2} \quad \text{and} \quad \|A\mathbf{U}\|_{\mathcal{C}} \le R.$$

The contraction-mapping theorem can be applied to establish the local existence of a solution of (8).

For uniqueness, let $\mathbf{H} = \mathbf{U} - \mathbf{W}$, where $\mathbf{U}$ and $\mathbf{W}$ are two solutions of (8) in $\mathcal{C} = C(0, T_1; C(0, L))^2$. As in (12), one can show that

$$\|\mathbf{H}\|_{\mathcal{C}} \le C \int_0^t \|\mathbf{H}\|_{\mathcal{C}}\, d\tau$$

for $0 \le t \le T_1$, where C depends on both $\|\mathbf{U}\|_C$ and $\|\mathbf{W}\|_C$. Gronwall's lemma then implies that

$$\|\mathbf{H}\|_C = 0,$$

which finishes the proof of the theorem. □

Theorem 3 (*(Regularity)*). Let $\mathbf{f} = (f_1, f_2) \in C^2(0, L)^2$, $\mathbf{h} = (h_1, h_2)$, $\mathbf{v} = (v_1, v_2) \in C^1(0, T)^2$ for some T, $L > 0$ satisfy the compatibility conditions (6). Then any solution pair (N, W) in $C(0, T_0; C(0, L))^2$ of (8) lies in $C^1(0, T_0; C^2(0, L))^2$ and is a classical solution of the initial- and boundary-value problem (4) on the interval $[0, T_0]$.

Proof. Since $\mathbf{U} \equiv (N, W)$ has continuous component functions, one shows by using Lemma 1(b) that $A\mathbf{U}$ is differentiable with respect to t, whence $\mathbf{U}_t$ exists and is given by (7). Since $\mathbf{h}'$ and $\mathbf{v}' \in C^0(0, T)^2$, it transpires that $\mathbf{U}_t \in C$. Rewrite (8) as

$$N = f_1(x) + \int_0^t \mathcal{M}(W + NW)\,d\tau + S(L - x)(h_1(t) - h_1(0)) + S(x)(h_2(t) - h_2(0)),$$

$$W = f_2(x) + \int_0^t \mathcal{M}(N + \tfrac{1}{2}WW)\,d\tau + S(L - x)(v_1(t) - v_1(0)) + S(x)(v_2(t) - v_2(0)),$$

where $\mathcal{M}$ is defined in (9). Lemma 1 yields that the terms on the right-hand side of the latter equations are in $C^1(0, T_0; C^1(0, L))$, which is equivalent to saying that N and W are in $C^1(0, T_0; C^1(0, L))$. Using the same argument once more gives that $(N, W) \in C^1(0, T_0; C^2(0, L))^2$.

Using (8) again shows that (5) is valid because $S(0) = 0$, $S(L) = 1$, and $K(0, s) = K(L, s) = 0$. That the solution of (8) satisfies (4) can be established by observing that the derivation leading from (4) to (8) is reversible if $(N, W) \in C^1(0, T_0; C^2(0, L))^2$. □

Theorem 4 (*(More regularity of the solution)*). Let $\mathbf{f} = (f_1, f_2) \in C^l(0, L)^2$, $\mathbf{h} = (h_1, h_2)$, $\mathbf{v} = (v_1, v_2) \in C^k(0, T)^2$ for some T, $L > 0$, $l \ge 2$, $k \ge 1$, satisfy the compatibility conditions (6). Then any solution pair (N, W) in $C(0, T_0; C(0, L))^2$ lies in $C^k(0, T_0; C^l(0, L))^2$ and is the classical solution of the initial- and boundary-value problem (4) on the interval $[0, T_0]$.

Proof. This results from a straightforward extension of the argument in the proof of Theorem 3. □

Definition. A polynomial $P(x_1, \ldots, x_n)$ is said to have degree l_j in the variable x_j if when all the other variables are held fixed, P is a polynomial of degree at most l_j.

Denote the boundary terms h_1, h_2, v_1, v_2, by Φ; i.e. $\Phi = (\phi_1, \phi_2, \phi_3, \phi_4) \equiv (h_1, h_2, v_1, v_2)$. By $\|\Phi(t)\|$ we mean $\max_{1 \le i \le 4} |\phi_i(t)|$. Bounds are now derived for the temporal and spatial derivatives of N and W in terms of bounds for N and W.

Theorem 5 (*(Bounds on solutions of (4))*). Let $\mathbf{f} = (f_1, f_2) \in C^l(0, L)^2$, $\Phi \in C^1(0, T)^4$, for some T, $L > 0$, $l \ge 2$, and suppose the compatibility conditions (6) to be satisfied. Let $T_0 > 0$ and let (N, W) be the solution of (4) corresponding to the auxiliary data $\mathbf{f}$ and Φ. For $k \le l$ a positive integer, define

$$\sigma_k(t) = \max_{\tau \in [0,t]} \max \left\{ \left\| \frac{\partial^k N(x, T)}{\partial x^k} \right\|, \left\| \frac{\partial^k W(x, T)}{\partial x^k} \right\| \right\},$$

and

$$B^1(t) = \max_{0\le\tau\le t}\{\|\Phi(\tau)\|\}, \qquad \|\mathbf{f}\|_k = \max_{0\le j\le k}\|\mathbf{f}^{(j)}\|.$$

Then for $t \in [0, T_0]$,

$$\sigma_k(t) \le P_k(B^1(t), \|\mathbf{f}\|_k, \sigma_0(t)),$$

where P_k can be bounded by a polynomial of degree k in $B^1(t)$ and $\|\mathbf{f}\|_k$ and of degree $k+1$ in $\sigma_0(t)$ with coefficients depending on k, L and T_0.

Proof. From (8), one verifies that for any $t > 0$,

$$\begin{aligned} N_x(x,t) &= f_1'(x) + \frac{\mathrm{d}}{\mathrm{d}x}\int_0^t\int_0^L K(x,s)(W+NW)\,\mathrm{d}s\,\mathrm{d}r \\ &\quad - S'(L-x)(h_1(t)-h_1(0)) + S'(x)(h_2(t)-h_2(0)), \\ W_x(x,t) &= f_2'(x) + \frac{\mathrm{d}}{\mathrm{d}x}\int_0^t\int_0^L K(x,s)(N+\tfrac{1}{2}W^2)\,\mathrm{d}s\,\mathrm{d}r \\ &\quad - S'(L-x)(v_1(t)-v_1(0)) + S'(x)(v_2(t)-v_2(0)). \end{aligned}$$

Using Lemma 1(b) and the fact that $|S(x)| \le 1$ for $|x| \le L$, it is seen that

$$\begin{aligned} \|N_x\| &\le \|\mathbf{f}\|_1 + T_0 D_0\|W + NW\| + 4\|S'(x)\|B^1(t), \\ \|W_x\| &\le \|\mathbf{f}\|_1 + T_0 D_0\|N + \tfrac{1}{2}W^2\| + 4\|S'(x)\|B^1(t), \end{aligned}$$

which yields

$$\max\{\|N_x\|, \|W_x\|\} \le P_1(B^1(t), \|\mathbf{f}\|_1, \sigma_0(t)).$$

Bounds for higher-order spatial derivatives can be obtained inductively using a similar argument and Lemma 1(b). □

3. The numerical scheme

The numerical scheme is based on the integral equations (7). Finite-difference schemes can also be used to approximate solutions of the system (4). If these are employed, proper treatment of the boundary conditions would be required to achieve high-order accuracy in both space and time. As will appear presently, the imposition of the boundary conditions in such a way that high-order overall accuracy is achieved is very simple when the scheme is based on (7).

We turn now to the details of the scheme. Let Δt be the step-size for the temporal discretization and Δx the length of the spatial discretization; let $(M+1)$ be the number of spatial mesh points so that $M\Delta x = L$. The equations in (7) are first discretized in space via numerical quadrature; the resultant system of ordinary differential equations are then integrated forward in time by a finite-difference, predictor–corrector method. The resulting scheme is fourth-order accurate in time and space, and we will show that for each time step, the only computational work involved is to solve a trigiagonal system, which requires order M operations where M is as above.

3.1. Spatial discretization

The spatial discretization is effected by approximating $\phi(x_i) = \int_0^L K(x_i, s)y(s)\,ds$, $i = 0, 1, \ldots, M$, by the trapezoidal rule with boundary corrections,

$$\int_{j\Delta x}^{k\Delta x} y(x)\,dx \approx I_{j,k}(y) \equiv \Delta x\left[\frac{1}{2}(y(j\Delta x^+) + y(k\Delta x^-)) + \sum_{i=j+1}^{k-1} y(i\Delta x)\right] + \tfrac{1}{12}\Delta x^2(y'(j\Delta x^+) - y'(k\Delta x^-)).$$

This approximation is of order 4 when $y \in C^4(j\Delta x, k\Delta x)$. Taking account of the fact that $K(x, s)$ is discontinuous at $x = s$ and denoting $K(x_i, s) = K_i(s)$, one has that

$$\begin{aligned}\phi(x_i) &= \int_0^L K_i(s)y(s)\,ds \approx L_i(y)\\ &\equiv \tfrac{1}{2}\Delta x[K_i(0)y(0) + (K_i(i\Delta x^-) + K_i(i\Delta x^+))y(i\Delta x) + K_i(L)y(L)]\\ &\quad + \Delta x\sum_{j=1, j\neq i}^{M-1} K_i(j\Delta x)y(j\Delta x) + \frac{1}{12}\Delta x^2[(K_i(s)y(s))'|_{0+}\\ &\quad - (K_i(s)y(s))'|_{i\Delta x-} + (K_i(s)y(s))'|_{i\Delta x+} - (K_i(s)y(s))'|_{M\Delta x-}].\end{aligned}$$

Writing $K(x, s) = K^1(x, s) + K^2(x, s)$ with

$$K^1(x, s) = \tfrac{1}{2}a^2 S(L - x - s), \qquad K^2(x, s) = \tfrac{1}{2}a^2\,\mathrm{sign}(x - s)S(L - |x - s|),$$

and after some simple computation, one obtains for $i = 1, 2, \ldots, M - 1$ that

$$L_i(y) = F_i^1 + F_i^2 + F_i^0 - \tfrac{1}{12}a^2\Delta x^2 y'(i\Delta x),$$

where

$$\begin{aligned}F_i^1 &= \Delta x\sum_{j=1}^{M-1}(K_i^1(j\Delta x)y(j\Delta x)),\\ F_i^2 &= \Delta x\sum_{j=1}^{M-1}(K_i^2(j\Delta x)y(j\Delta x)) \quad \text{with } K_i^2(i\Delta x) = 0,\\ F_i^0 &= \tfrac{1}{2}a^2\Delta x[y(0)s_{M-i} - y(L)s_i] + \tfrac{1}{12}a^2\Delta x^2[y'(0)s_{M-i} + y'(L)s_i],\end{aligned}$$

and

$$s_i = S(i\Delta x), \quad \text{for } i = 0, 1, \ldots, M.$$

The derivatives $y'(0)$, $y'(L)$ and $y'(i\Delta x)$ in $L_i(y)$ may be replaced by the finite differences

$$\begin{aligned}y'(0) &\approx \frac{1}{2\Delta x}(-y(2\Delta x) + 4y(\Delta x) - 3y(0)),\\ y'(L) &\approx \frac{1}{2\Delta x}(y(L - 2\Delta x) - 4y(L - \Delta x) + 3y(L)),\end{aligned}$$

and

$$y'(i\Delta x) \approx \frac{1}{2\Delta x}(y((i+1)\Delta x) - y((i-1)\Delta x)),$$

for $i = 1, 2, \ldots, M-1$. Write $y_i = y(i\Delta x)$ so that $\phi(x_i) \equiv \int_0^L K(x_i, s)y(s)\,ds$ is approximated by

$$\phi_i(\mathbf{y}) \equiv F_i^1 + F_i^2 + \tilde{F}_i^0 - \tfrac{1}{24}a^2\Delta x^2(y_{i+1} - y_{i-1}), \tag{13}$$

where $\mathbf{y} = (y_0, \ldots, y_M)$ and

$$\begin{aligned}\tilde{F}_i^0 &= \tfrac{1}{2}a^2\Delta x[y_0 s_{M-i} - y_M s_i] \\ &\quad + \tfrac{1}{24}a^2\Delta x[(-y_2 + 4y_1 - 3y_0)s_{M-i} + (y_{M-2} - 4y_{M-1} + 3y_M)s_i].\end{aligned}$$

Applying these spatial discretizations to (7) and denoting $\mathbf{W} = (W_0, \ldots, W_M)$ and $\mathbf{N} = (N_0, \ldots, N_M)$ where $W_i = W(i\Delta x, t)$, $N_i = N(i\Delta x, t)$, $N_t(x_i, t)$ and $W_t(x_i, t)$ can be approximated by

$$\begin{aligned}N_t(x_i, t) &\approx \phi_i(\mathbf{W} + \mathbf{N} \circ \mathbf{W}) + S(L - x_i)h_1' + S(x_i)h_2', \\ W_t(x_i, t) &\approx \phi_i(\mathbf{N} + \tfrac{1}{2}\mathbf{W} \circ \mathbf{W}) + S(L - x_i)v_1' + S(x_i)v_2'.\end{aligned}$$

The symbol $\mathbf{N} \circ \mathbf{W}$ denotes the componentwise product of $\mathbf{N}$ and $\mathbf{W}$, which is to say $\mathbf{N} \circ \mathbf{W} = (N_0W_0, \ldots, N_MW_M)$.

The semi-discrete algorithm is then to find vectors $\mathbf{n} = (n_0(t), \ldots, n_M(t))$ and $\mathbf{w} = (w_0(t), \ldots, w_M(t))$ which are approximations to N and W, respectively, such that for $i = 1, \ldots, M-1$,

$$\begin{aligned}&(n_i)_t = \phi_i(\mathbf{f}_n) + s_{M-i}h_1' + s_i h_2', \qquad (w_i)_t = \phi_i(\mathbf{f}_w) + s_{M-i}v_1' + s_i v_2', \\ &n_0 = h_1, \quad n_M = h_2, \qquad w_0 = v_1, \quad w_M = v_2,\end{aligned} \tag{14}$$

where $\mathbf{f}_n = \mathbf{w} + \mathbf{n} \circ \mathbf{w}$ and $\mathbf{f}_w = \mathbf{n} + \frac{1}{2}\mathbf{w} \circ \mathbf{w}$. Denoting $\hat{\mathbf{n}} = (n_1, \ldots, n_{M-1})$ and $\hat{\mathbf{w}} = (w_1, \ldots, w_{M-1})$, and identifying n_0, n_M, w_0, w_M as h_1, h_2, v_1, v_2, the system (14) may be written as the system of ordinary differential equations

$$\frac{\mathrm{d}}{\mathrm{d}t}\begin{pmatrix}\hat{\mathbf{n}} \\ \hat{\mathbf{w}}\end{pmatrix} = \begin{pmatrix}\mathbf{f}_1(t, \hat{\mathbf{n}}, \hat{\mathbf{w}}) \\ \mathbf{f}_2(t, \hat{\mathbf{n}}, \hat{\mathbf{w}})\end{pmatrix} \quad \text{or} \quad \frac{\mathrm{d}}{\mathrm{d}t}\mathbf{u} = \mathbf{f}(t, \mathbf{u}), \tag{15}$$

where $\mathbf{u} \equiv (\hat{\mathbf{n}}, \hat{\mathbf{w}})^{\mathrm{T}}$ and $\mathbf{f}(t, \mathbf{u}) \equiv (\mathbf{f}_1(t, \hat{\mathbf{n}}, \hat{\mathbf{w}}), \mathbf{f}_2(t, \hat{\mathbf{n}}, \hat{\mathbf{w}}))^{\mathrm{T}}$. Observing that the dependence of $\mathbf{f}_1$ and $\mathbf{f}_2$ on the boundary terms $\Phi = (h_1, h_2, v_1, v_2)$ is separate from their dependence on $\hat{\mathbf{n}}$ and $\hat{\mathbf{w}}$, we write (see (13))

$$\begin{aligned}\mathbf{f}_1(t, \hat{\mathbf{n}}, \hat{\mathbf{w}}) &\equiv L_N(\hat{\mathbf{w}} + \hat{\mathbf{n}} \circ \hat{\mathbf{w}}) + B_N(\Phi, \Phi'), \\ \mathbf{f}_2(t, \hat{\mathbf{n}}, \hat{\mathbf{w}}) &\equiv L_N(\hat{\mathbf{n}} + \tfrac{1}{2}\hat{\mathbf{w}} \circ \hat{\mathbf{w}}) + B_W(\Phi, \Phi'),\end{aligned} \tag{16}$$

where L_N is a matrix independent of $\hat{\mathbf{n}}$, $\hat{\mathbf{w}}$, and $B_N(\Phi, \Phi')$ and $B_W(\Phi, \Phi')$ are vectors whose components are polynomials quadratic in the components of Φ and Φ'.

3.2. Acceleration procedure

If $M+1$ is the number of spatial mesh points, a direct evaluation of $\phi_i(\mathbf{y})$, $i = 0, 1, \ldots, M$, will involve on the order of M^2 operations. To reduce the computation to order M operations, we follow the scheme put forward in [4,5] by defining

$$(D^2\mathbf{y})_i = y_i - (y_{i+1} - 2y_i + y_{i-1})/(\mathrm{e}^{a\Delta x} - 2 + \mathrm{e}^{-a\Delta x}) \equiv Ay_i + B(y_{i+1} + y_{i-1}),$$

where

$$B = \frac{-1}{e^{a\Delta x} - 2 + e^{-a\Delta x}} \quad \text{and} \quad A = 1 - 2B.$$

Notice that if $\mathbf{y} = (y_0, y_1, \ldots)$ and $y_i = e^{ai\Delta x}$, then

$$(D^2\mathbf{y})_i = 0 \quad \text{for all } i.$$

Denoting $\tilde{\mathbf{F}}^0 = (\tilde{F}_i^0)$, $\mathbf{F}^1 = (F_i^1)$ (see (13)), then since $e^{ax_i} = e^{ai\Delta x}$, it transpires that

$$(D^2\tilde{\mathbf{F}}^0)_i = 0, \quad i = 1, \ldots, M-1,$$
$$(D^2\tilde{\mathbf{F}}^1)_i = 0, \quad i = 1, \ldots, M-1.$$

Defining $\mathbf{K}$ by

$$K_{ij} = \operatorname{sign}(i-j)e^{a|i-j|\Delta x},$$

it is straightforward to verify that

$$\left(D^2\left(\sum_{j=1}^{m-1} K_{ij}y_j\right)\right)_i = \begin{cases} By_2, & i = 1, \\ B(y_{i+1} - y_{i-1}), & i = 2, 3, \ldots, M-2, \\ -By_{M-2}, & i = M-1. \end{cases}$$

In consequence, if $\mathbf{G} = \mathbf{F}^1 + \mathbf{F}^2 + \tilde{\mathbf{F}}^0$, where $\mathbf{G} = (G_i)$, $\mathbf{F}^2 = (F_i^2)$, then

$$(D^2\mathbf{G})_i = AG_i + B(G_{i+1} + G_{i-1}) = (D^2\mathbf{F}^2)_i$$
$$= \begin{cases} \frac{1}{2}a^2B\Delta x y_2, & i = 1, \\ \frac{1}{2}a^2B\Delta x(y_{i+1} - y_{i-1}), & i = 2, 3, \ldots, M-2, \\ -\frac{1}{2}a^2B\Delta x y_{M-2} & i = M-1. \end{cases}$$

To complete the system of equations for $G_1, \ldots, G_{M-1}$, observe that

$$AG_1 + BG_2 = -BG_0 + \tfrac{1}{2}a^2B\Delta x y_2,$$

where

$$G_0 = \tilde{F}_0^0 = \tfrac{1}{2}a^2\Delta x[y_0 + \tfrac{1}{12}(-y_2 + 4y_1 - 3y_0)]$$

and

$$AG_{M-1} + BG_{M-2} = -BG_M - \tfrac{1}{2}a^2B\Delta x y_{M-2},$$

with

$$G_M = \tilde{F}_M^0 = -\tfrac{1}{2}a^2\Delta x[y_M - \tfrac{1}{12}(y_{M-2} - 4y_{M-1} + 3y_M)].$$

Thus, evaluating $\phi_i(\mathbf{y})$, for $i = 1, 2, \ldots, M-1$, can be accomplished by solving the preceding tridiagonal linear system for $G_1, \ldots, G_{M-1}$, and then using (13) in the form

$$\phi_i(\mathbf{y}) = G_i - \tfrac{1}{2}a^2\Delta x(y_{i+1} - y_{i-1})$$

for $i = 1, \ldots, M-1$. The total operation count for this procedure is of order M, which is optimal.

It is easy to verify that $w_0 = w_M = 0$ because

$$K_0^1(s) = -K_0^2(s) \quad \text{and} \quad K_M^1(s) = -K_M^2(s).$$

3.3. Temporal discretization

The Adams fourth-order predictor–corrector scheme, (P_4EC_4E) in the parlance of Isaacson and Keller [19], is used for the integration of (15) in time. In case the exact values of the boundary terms $\Phi'(t)$ are not available, they are calculated via the fourth-order central difference formula

$$\Phi'(l\Delta t) \approx \mathrm{d}\Phi' \equiv \frac{1}{12\Delta t}(\Phi^{l-2} - 8\Phi^{l+1} - \Phi^{l+2}), \tag{17}$$

where $\Phi^l = \Phi(l\Delta t)$, $l \in \mathbb{N}$. Let $\mathbf{f}^l(\mathbf{u})$ denote the function obtained by approximating $\Phi'(l\Delta t)$ with $\mathrm{d}\Phi^l$ in $\mathbf{f}(l\Delta t, \mathbf{u})$ (i.e. replacing $B_N(\Phi, \Phi')$) and $B_W(\Phi, \Phi')$ by $B_N(\Phi, \mathrm{d}\Phi)$ and $B_w(\Phi, \mathrm{d}\Phi)$, respectively). The numerical scheme for $\mathbf{u}$ is

$$\begin{aligned}
\tilde{\mathbf{u}}^{l+1} &= \mathbf{u}^l + \tfrac{1}{24}\Delta t[55\mathbf{f}^l(\mathbf{u}^l) - 59\mathbf{f}^{l-1}(\mathbf{u}^{l-1}) + 37\mathbf{f}^{l-2}(\mathbf{u}^{l-2}) - 9\mathbf{f}^{l-3}(\mathbf{u}^{l-3})],\\
\tilde{\mathbf{u}}^{l+1} &= \mathbf{u}^l + \tfrac{1}{24}\Delta t[9\mathbf{f}^{l+1}(\tilde{\mathbf{u}}^{l+1}) + 19\mathbf{f}^l(\mathbf{u}^l) + 5\mathbf{f}^{l-1}(\mathbf{u}^{l-1}) + \mathbf{f}^{l-2}(\mathbf{u}^{l-2})].
\end{aligned} \tag{18}$$

The fourth-order Runge–Kutta–Simpson method can be used for the first three steps to generate the starting values for the Adams method whenever it is necessary. The fourth-order predictor–corrector scheme was employed because it requires two-functional evaluation instead of four when compared with the fourth-order Runge–Kutta scheme. The advantage in stability of the fourth-order Runge–Kutta scheme for the ordinary differential equation is not important because the system is not stiff. Indeed, we will show presently that our scheme is unconditionally stable.

Remarks.

(i) The same method can be used to develop schemes of arbitrary order of accuracy by using higher-order derivative corrections for the trapezoidal rule (i.e. the Euler–Maclaurin formula) and higher-order prediction–correction time stepping methods.

(ii) In some of our computations, the initial Runge–Kutta steps can be avoided. This situation is obtained when we are approximating a known, exact solution or in cases where the disturbance comes entirely through the boundary, so that zero initial conditions are appropriate.

4. Analysis of the numerical scheme

In this section, we prove that the algorithm (18) is fourth-order accurate in time and in space, and that it is unconditionally stable.

Lemma 6 (*(Error for the Trapezoidal rule with boundary correction)*). If $y \in C^4(j\Delta x, k\Delta x)$, then

$$\int_{j\Delta x}^{k\Delta x} y(x)\,\mathrm{d}x - I_{j,k}(y) = \frac{\Delta x^4}{384}\int_{j\Delta x}^{k\Delta x} |y^{(4)}(x)|\,\mathrm{d}x.$$

Proof. This is a standard result (cf. [16]). □

Lemma 7 (*(Spatial discretization error)*). Let there be given $y \in C^4(0, L)$, a positive integer M and $\Delta x = L/M \leq 1$. Let $\mathbf{y} = (y_0, y_1, \ldots, y_M)$ where $y_i \equiv y(i\Delta x)$. Then for $i = 1, \ldots, M-1$,

$$\left|\phi_i(y) - \int_0^L K_i(s)y(s)\,\mathrm{d}s\right| \le c_2 M_4 \Delta x^4,$$

where $M_4 = \max_{0\le j\le 4}\{\|y^{(j)}(x)\|\}$ and c_2 is a constant depending only on L.

Proof. By the definition of $\phi_i(\mathbf{y})$ and using Lemma 6, one finds that

$$\begin{aligned}
&\left|\phi(\mathbf{y}) - \int_0^L K_i(s)y(s)\,\mathrm{d}s\right| \\
&\quad\le \left|L_i(y) - \int_0^L K_i(s)y(s)\,\mathrm{d}s\right| + |L_i(y) - \phi_i(\mathbf{y})| \\
&\quad\le \frac{\Delta x^4}{384}\left(\int_0^{i\Delta x} |(K_i\cdot y)^{(4)}(s)|\,\mathrm{d}s + \int_{i\Delta x}^{L} |(K_i\cdot y)^{(4)}(s)|\,\mathrm{d}s\right) \\
&\qquad + \frac{a^2\Delta x^2}{12}\left\{\left|y'(i\Delta x) - \frac{y_{i+1}-y_{i-1}}{2\Delta x}\right| + |s_{M-i}|\left|y'(0) - \frac{-y_2+4y_1-3y_0}{2\Delta x}\right| + |s_i|\left|y'(L)\right.\right. \\
&\qquad\qquad \left.\left. - \frac{y_{M-2}-4y_{M-1}+3y_M}{2\Delta x}\right|\right\}.
\end{aligned}$$

Applying Lemma 1(a) to the first two terms, the conclusion emerges. □

We will denote the max-norm of a vector $\mathbf{y}$ by $|\mathbf{y}|$.

Lemma 8 ((Lipschitz condition for the mapping $\mathbf{f}$ *in* Eq. (15))).

(a) The functions $\phi_i(\mathbf{y})$ are Lipschitz, $i = 1, \ldots, M-1$; i.e. for any $\mathbf{y}, \mathbf{z} \in \mathbb{R}^{M+1}$,

$$\max_{1\le i\le M-1} |\phi_i(\mathbf{y}) - \phi_i(\mathbf{z})| \le C_L|\mathbf{y}-\mathbf{z}|,$$

where C_L is a constant depending only on L.

(b) The max-norm of the matrix L_N in (16) is bounded, which is to say there is a contant C_L depending only on L such that

$$\|L_N\|_\infty \le C_L.$$

(c) For fixed $\Phi \in C^1(0,T)^4$, $\mathbf{f}(t,\mathbf{u})$ is uniformly Lipschitz continuous on bounded subsets of l_∞. More precisely, for any $\mathbf{u}_1, u_2 \in \mathbb{R}^{2M-2}$, there is a constant C_L depending on L, but not on $\mathbf{u}_1$, $\mathbf{u}_2$ or M, so that

$$|\mathbf{f}(t,\mathbf{u}_1) - \mathbf{f}(t,\mathbf{u}_2)| \le C_L(1 + |\mathbf{u}_1| + |\mathbf{u}_2|)|\mathbf{u}_1 - \mathbf{u}_2|.$$

Proof. From (13), validating part (a) only requires estimating the max-norm of the matrix $\Delta x K^l$, with $K^l(i,j) = K_i^l(j\Delta x)$, $l = 1, 2$. A simple calculation shows that $\Delta x\|K^l\|_\infty$ is bounded by a constant depending only on L, and (a) is proved.

Let $\hat{\mathbf{y}} = (y_1, \ldots, y_{M-1})$, $\tilde{\mathbf{y}} = (0, \hat{\mathbf{y}}, 0)$, and similarly, let $\hat{\mathbf{z}} = (z_1, \ldots, z_{M-1})$, $\tilde{\mathbf{z}} = (0, \hat{\mathbf{z}}, 0)$. Since

$$(L_N\hat{\mathbf{y}})_i = \phi_i(\tilde{\mathbf{y}}),$$

it follows that

$$|L_N\hat{\mathbf{y}} - L_N\hat{\mathbf{z}}| \le C_L|\tilde{\mathbf{y}} - \tilde{\mathbf{z}}| = C_L|\hat{\mathbf{y}} - \hat{\mathbf{z}}|,$$

which yields (b).

For (c), write $\mathbf{u}_1$ and $\mathbf{u}_2$ as $\mathbf{u}_1 = (\mathbf{n}_1, \mathbf{w}_1)$, $\mathbf{u}_2 = (\mathbf{n}_2, \mathbf{w}_2)$, and observe that

$$\mathbf{f}(t, \mathbf{u}_1) - \mathbf{f}(t, \mathbf{u}_2) = \begin{pmatrix} L_N(\hat{\mathbf{w}}_1 + \hat{\mathbf{n}}_1 \circ \hat{\mathbf{w}}_1) - L_N(\hat{\mathbf{w}}_2 + \hat{\mathbf{n}}_2 \circ \hat{\mathbf{w}}_2) \\ L_N(\hat{\mathbf{w}}_1 + \frac{1}{2}\hat{\mathbf{w}}_1 \circ \hat{\mathbf{w}}_1) - L_N(\hat{\mathbf{w}}_2 + \frac{1}{2}\hat{\mathbf{w}}_2 \circ \hat{\mathbf{w}}_2) \end{pmatrix}.$$

Using part (b), there appears

$$\begin{aligned} |\mathbf{f}(t, \mathbf{u}_1) - \mathbf{f}(t, \mathbf{u}_2)| &\le \begin{pmatrix} C_L|\hat{\mathbf{w}}_1 - \hat{\mathbf{w}}_2 + \hat{\mathbf{n}}_1 \circ \hat{\mathbf{w}}_1 - \hat{\mathbf{n}}_2 \circ \hat{\mathbf{w}}_2| \\ C_L|\hat{\mathbf{n}}_1 - \hat{\mathbf{n}}_2 + \frac{1}{2}\hat{\mathbf{w}}_1 \circ \hat{\mathbf{w}}_1 - \frac{1}{2}\hat{\mathbf{w}}_2 \circ \hat{\mathbf{w}}_2| \end{pmatrix} \\ &\le C_L(1 + |\mathbf{u}_1| + |\mathbf{u}_2|)|\mathbf{u}_1 - \mathbf{u}_2|. \qquad \square \end{aligned}$$

Suppose $[0, T_0]$ is a temporal interval over which we have existence of a solution as discussed in Theorem 2. Using Theorem 4, one infers that if $l \ge 2$ and $k \ge 1$, then for initial data $f_1, f_2 \in C^l(0, L)$ and boundary data $\phi_i \in C^k(0, T)$ for $i = 1, \ldots, 4$, satisfying the compatibility conditions (6), the unique solution (N, W) in $C(0, T_0; C(0, L))^2$ of (7) lies in $C^k(0, T_0; C^l(0, L))^2$ and is the classical solution of the initial- and boundary-value problem (4) and (5) on the interval $[0, T_0]$.

For simplicity of exposition, we will assume from now on that the initial data $(f_1, f_2) = \mathbf{0}$. The conclusions remain valid for non-zero initial data satisfying $f_1, f_2 \in C^4(0, L)$ and the compatibility conditions (6).

Lemma 9 ((Local truncation error)). Let $N, W \in C(0, T_0; C^4(0, L))$ be the solution of (4) and (5) and let $N_i(t) = N(i\Delta x, t)$, $W_i(t) = W(i\Delta x, t)$, $i = 1, 2, \ldots, M-1$, where M and Δx are as in Lemma 7. Define $\mathbf{U} = (N_1, \ldots, N_{M-1}, W_1, \ldots, W_{M-1})$. Then for $0 \le t \le T_0$,

$$\left|\frac{\mathrm{d}}{\mathrm{d}t}\mathbf{U} - \mathbf{f}(t, \mathbf{U})\right| \le c_2\Delta x^4 Q_1(\sigma_0(t), \ldots, \sigma_4(t)) \equiv e_1(t),$$

where Q_1 is a quadratic polynomial in the quantities σ_i introduced in Theorem 5 ($i = 0, 1, \ldots, 4$) with numerical coefficients and c_2 is the constant appearing in Lemma 7 which depends only on L.

Proof. Let $N = (N_0, \ldots, N_M)$ and $\mathbf{W} = (W_0, \ldots, W_M)$. From the equations in (7), and using Lemma 7, one finds

$$\begin{aligned} &\left|\frac{\mathrm{d}}{\mathrm{d}t}\mathbf{U} - \mathbf{f}(t, \mathbf{U})\right| \\ &= \left|\begin{pmatrix} [\mathcal{F}_1(t, N, W)]_{x=x_1,\ldots,x_{M-1}} - \mathbf{f}_1(t, \hat{\mathbf{N}}, \hat{\mathbf{W}}) \\ [\mathcal{F}_2(t, N, W)]_{x=x_1,\ldots,x_{M-1}} - \mathbf{f}_2(t, \hat{\mathbf{N}}, \hat{\mathbf{W}}) \end{pmatrix}\right| \\ &= \left|\begin{pmatrix} [\int_0^L K_i(s)(W + NW)\,\mathrm{d}s - \phi_i(\mathbf{W} + \mathbf{N} \circ \mathbf{W})]_{i=1,\ldots,M-1} \\ [\int_0^L K_i(s)(W + \frac{1}{2}W^2)\,\mathrm{d}s - \phi_i(\mathbf{N} + \frac{1}{2}\mathbf{W} \circ \mathbf{W})]_{i=1,\ldots,M-1} \end{pmatrix}\right| \\ &\le c_2\Delta x^4 \max_{0\le j<4} \max\left\{\left\|\frac{\partial^{(j)}}{\partial x}(W + NW)\right\|, \left\|\frac{\partial^{(j)}}{\partial x}(N + \tfrac{1}{2}W^2)\right\|\right\}, \end{aligned}$$

which yields the advertised conclusion. $\square$

Lemma 10 ((*Existence and bounds for the solution of* (16))).
(a) Assume $\Phi \in C^1(0, T)^4$ and define

$$T_1 = \sup\{t_0 \mid T_0 \geq t_0 \geq 0 \text{ and } \mathbf{u}(t) \text{ exists with } |\mathbf{u}(t) - \mathbf{U}(t)| \leq 1 \quad \text{for } t \in [0, t_0]\}, \tag{19}$$

where $\mathbf{u}(t)$ is the solution of (15) and $\mathbf{U}(t)$ is defined as in Lemma 9. Then $T_1 \to T_0$ as $\Delta x \to 0$ and

$$|\mathbf{u}(t)| \leq 1 + \sigma_0(t) \quad \text{for } t \in [0, T_1],$$

where, as in Theorem 5,

$$\sigma_0(t) = \max_{\tau \in [0,t]} \max\{\|N(\cdot, \tau)\|, \|W(\cdot, \tau)\|\}$$

and the unadorned norm $\|\cdot\|$ is as before that of $C(0, L)$.
(b) If $\Phi \in C^k(0, T)^4$ and $k \geq 1$, then

$$\left|\frac{\mathrm{d}^k}{\mathrm{d}t^k}\mathbf{u}(t)\right| \leq Q_k(1 + \sigma_0(t), \Phi, \Phi', \ldots, \Phi^{(k)}) \quad \text{for } t \in [0, T_1],$$

where Q_k is a polynomial of degree at most $k + 1$.

Proof. Since $\mathbf{f}$ is locally Lipschitz continuous, there is a unique solution $\mathbf{u}(t)$ to (15) for $t \in [0, t_0]$, at least for some $t_0 > 0$. Since $\mathbf{u}(0) = \mathbf{U}(0) = \mathbf{0}$ and both $\mathbf{u}, \mathbf{U}$ are continuous, then $T_1 > 0$. We shall now obtain a lower bound for T_1 and show that $T_1 \to T_0$ as $\Delta x \to 0$. For $t \in [0, T_1]$, one has

$$\begin{aligned}\left|\frac{\mathrm{d}}{\mathrm{d}t}\mathbf{u}(t) - \frac{\mathrm{d}}{\mathrm{d}t}\mathbf{U}(t)\right| &= \left|f(t, \mathbf{u}) - \frac{\mathrm{d}}{\mathrm{d}t}\mathbf{U}(t)\right| \\ &\leq |\mathbf{f}(t, \mathbf{u}) - \mathbf{f}(t, \mathbf{U})| + \left|\mathbf{f}(t, \mathbf{U}) - \frac{\mathrm{d}}{\mathrm{d}t}\mathbf{U}(t)\right| \\ &\leq C_L(1 + |\mathbf{u}| + |\mathbf{U}|)|\mathbf{u} - \mathbf{U}| + e_1(t),\end{aligned}$$

where

$$e_1(t) = \max_{0 \leq s \leq t}\left|f(s, \mathbf{U}(s)) - \frac{\mathrm{d}}{\mathrm{d}s}\mathbf{U}(s)\right|.$$

In consequence, it transpires that

$$\left|\frac{\mathrm{d}}{\mathrm{d}t}\mathbf{u}(t) - \frac{d}{\mathrm{d}t}\mathbf{U}(t)\right| \leq 2C_L(1 + \sigma_0(t))|\mathbf{u} - \mathbf{U}| + e_1(t). \tag{20}$$

Because $(\mathrm{d}/\mathrm{d}t)|\mathbf{u}-\mathbf{U}| \leq (\mathrm{d}/\mathrm{d}t)(\mathbf{u}-\mathbf{U})$ except on a set of zero measure, and since $\sigma_0(t)$ and $e_1(t)$ are non-decreasing functions of t, it follows from Gronwall's lemma that

$$|\mathbf{u} - \mathbf{U}| \leq e_1(t)[\mathrm{e}^{2C_L(1+\sigma_0(t))t} - 1]/(2C_L(1 + \sigma_0(t))) \equiv \psi(t) \tag{21}$$

for $t \in [0, T_1]$.

It T_1 were such that $\psi(T_1) < 1$ and $T_1 < T_0$, it would contradict the maximality of T_1 in the definition (9) as follows, In this case, there is a t_2 with $0 < T_2 < T_0 - T_1$, such that $\mathbf{u}(t)$ is still defined and $|\mathbf{u} - \mathbf{U}| \leq 1$ for $t \in [T_1, T_1 + t_2]$, because $\mathbf{f}$ is locally Lipschitz continuous. Since $e_1(t)$ and $\sigma_0(t)$ are non-decreasing in t (let $e_1(t) = e_1(T_0), \sigma_0(t) = \sigma_0(T_0)$ for $t > T_0$), it follows that $\psi(t)$ is strictly increasing in t as soon as $e_1(t) > 0$. Since

$\sigma_0(t)$ and $e_1(t)$ are continuous, $\psi(t)$ is continuous and $\psi(t) \to \infty$ as $t \to \infty$. Thus it follows that $T_1 \geq \min\{T_0, \bar{T}\}$, where $\bar{T}$ is the unique solution of

$$\psi(\bar{T}) = 1.$$

Note that since $e_1(t) \to 0$ as $\Delta x \to 0$, $\bar{T} \to \infty$ as $\Delta x \to 0$. Thus $\mathbf{u}$ exists on an interval $[0, T_1]$ that coincides with $[0, T_0]$ for Δx sufficiently small. Moreover,

$$|\mathbf{u}(t)| \leq |\mathbf{u}(t) - \mathbf{U}(t)| + |\mathbf{U}(t)| \leq 1 + \sigma_0(t) \quad \text{for } t \in [0, T_1].$$

This finishes the proof of (a).

From (16) and (17), one has

$$\frac{\mathrm{d}}{\mathrm{d}t}\mathbf{u} = \begin{pmatrix} L_N(\hat{\mathbf{w}} + \hat{\mathbf{n}} \circ \hat{\mathbf{w}}) \\ L_N(\hat{\mathbf{n}} + \frac{1}{2}\hat{\mathbf{w}} \circ \hat{\mathbf{w}}) \end{pmatrix} + \begin{pmatrix} B_N(\phi, \phi') \\ B_W(\Phi, \Phi') \end{pmatrix},$$

where $\mathbf{u} = (\hat{\mathbf{n}}, \hat{\mathbf{w}})$. Since

$$\|L_N\|_\infty \leq C_L,$$

it is easy to see that

$$|L_N(\hat{\mathbf{w}} + \hat{\mathbf{n}} \circ \hat{\mathbf{w}})| \leq C_L(1 + |\mathbf{u}|)|\mathbf{u}|, \qquad |L_N(\hat{\mathbf{n}} + \tfrac{1}{2}\hat{\mathbf{w}} \circ \hat{\mathbf{w}})| \leq C_L(1 + |\mathbf{u}|)|\mathbf{u}|.$$

Observing that

$$|B_N(\Phi, \Phi')| \leq q_1(\Phi(t), \Phi'(t)), \qquad |B_W(\Phi, \Phi')| \leq q_1(\Phi(t), \Phi'(t)),$$

where q_1 is a quadratic polynomial in Φ and Φ', it is adduced that

$$\begin{aligned} \left|\frac{\mathrm{d}}{\mathrm{d}t}\mathbf{u}(t)\right| &\leq q_1(\Phi^{(0)}(t), \Phi^{(1)}(t)) + C_L(1 + |\mathbf{u}|)|\mathbf{u}| \\ &\equiv Q_1(|\mathbf{u}|, \Phi^{(0)}(t), \Phi^{(1)}(t)) \leq Q_1(1 + \sigma_0(t), \Phi^{(0)}(t), \Phi^{(1)}(t)), \end{aligned}$$

where Q_1 is a quadratic polynomial.

Since

$$\frac{\mathrm{d}^2\mathbf{u}}{\mathrm{d}t^2} = \begin{pmatrix} L_N\left(\frac{\mathrm{d}}{\mathrm{d}t}\hat{\mathbf{w}} + \left(\frac{\mathrm{d}}{\mathrm{d}t}\hat{\mathbf{n}}\right) \circ \hat{\mathbf{w}} + \hat{\mathbf{n}} \circ \left(\frac{\mathrm{d}}{\mathrm{d}t}\hat{\mathbf{w}}\right)\right) \\ L_N\left(\frac{\mathrm{d}}{\mathrm{d}t}\hat{\mathbf{n}} + \left(\frac{\mathrm{d}}{\mathrm{d}t}\hat{\mathbf{w}}\right) \circ \hat{\mathbf{w}}\right) \end{pmatrix} + \begin{pmatrix} E_N(\Phi, \Phi', \Phi'') \\ E_N(\Phi, \Phi', \Phi'') \end{pmatrix},$$

where E_N and E_W are quadratic with respect to Φ, Φ', Φ'', the inequality in (b) is obtained for $k = 2$. Applying the same argument inductively, one obtains the inequality in (b) for general k. □

Remark. From (20) and (21), one can prove that

$$\left|\frac{\mathrm{d}^k}{\mathrm{d}t^k}[\mathbf{u}(t) - \mathbf{U}(t)]\right| \to 0$$

for any k and t as $\Delta x \to 0$.

Lemma 11 (*(Temporal discretization error)*). Let $T_1, \Delta t > 0$ be given and let $|\cdot|$ denote the max-norm on $\mathbb{R}^{2(M-1)}$. Suppose that $\mathbf{u} = \mathbf{u}(t) \in C^5(-3\Delta t, T_1)^{2(M-1)}$, $\mathbf{u}_t = \mathbf{f}(t, \mathbf{u})$ on the interval $[-3\Delta t, T_1]$ and $\mathbf{u} = \mathbf{0}$ on $[-3\Delta t, 0]$, where $\mathbf{f}(t, \mathbf{u})$ is Lipschitz continuous in $\mathbf{u}$ with Lipschitz constant K, which is to say

$$|\mathbf{f}(t, \mathbf{u}_1) - \mathbf{f}(t, \mathbf{u}_2)| \le K|\mathbf{u}_1 - \mathbf{u}_2|$$

for $\mathbf{u}_1, \mathbf{u}_2 \in \mathbb{R}^{2(M-1)}$ and $t \in (-3\Delta t, \bar{T})$. Let $\mathbf{u}^l$, $l \ge 1$ be determined by the iteration

$$\bar{\mathbf{u}}^l = \mathbf{u}^{l-1} + \tfrac{1}{24}\Delta t(55\mathbf{f}^{l-1} - 59\mathbf{f}^{l-2} + 37\mathbf{f}^{l-3} - 9\mathbf{f}^{l-4}) + \Delta t\bar{\theta}^l,$$
$$\mathbf{u}^l = \mathbf{u}^{l-1} + \tfrac{1}{24}\Delta t(9\bar{\mathbf{f}}^l + 19\mathbf{f}^{l-1} - 5\mathbf{f}^{l-2} + \mathbf{f}^{l-3}) + \Delta t\theta^l,$$

(which is equivalent to (19)), where $\mathbf{f}^j = \mathbf{f}(j\Delta t, \mathbf{u}^j)$, $\bar{\mathbf{f}}^j = \mathbf{f}(j\Delta t, \bar{\mathbf{u}}^j)$ and $\mathbf{u}^0 = \mathbf{u}^{-1} = \mathbf{u}^{-2} = \mathbf{u}^{-3} = 0$. Suppose that the errors θ^l and $\bar{\theta}^l$ satisfy

$$|\theta^l| + \tfrac{3}{8}K\Delta t|\bar{\theta}^l| \le \theta$$

for $l \le T_1/\Delta t$. Then for all $l \le T_1/\Delta t$, it follows that

$$|\mathbf{u}^l - \mathbf{u}(l\Delta t)| \le \left[c_3\left(1 + \frac{3}{8}K\Delta t\right)\Delta t^4 \sup_{t\in[0,T]}|\mathbf{u}^{(5)}(t)| + \theta\right]\frac{e^{c_d T_1} - 1}{c_d},$$

where $c_d = \frac{1}{12}K(17 + 30K\Delta t)$ and c_3 is a numerical constant.

Proof. This is a standard result (see [19]). □

To apply this lemma to the scheme (18), let $\bar{\theta}^l$ and θ^l be defined as

$$\bar{\theta}^l = \begin{pmatrix} \left(\frac{1}{24}\sum_{j=1}^4 \bar{a}_j h_1'((l-j)\Delta t) - \mathrm{d}h_1^{l-j}\right)\mathbf{z}^1 + \left(\frac{1}{24}\sum_{j=1}^4 \bar{a}_j h_2'((l-j)\Delta t) - \mathrm{d}h_2^{l-j}\right)\mathbf{z}^2 \\ \left(\frac{1}{24}\sum_{j=1}^4 \bar{a}_j v_1'((l-j)\Delta t) - \mathrm{d}v_1^{l-j}\right)\mathbf{z}^1 + \left(\frac{1}{24}\sum_{j=1}^4 \bar{a}_j v_2'((l-j)\Delta t) - \mathrm{d}v_2^{l-j}\right)\mathbf{z}^2 \end{pmatrix},$$

where $(\mathbf{z}^1)_i = s_{M-i}$, $(\mathbf{z}^2)_i = s_i$ for $i = 1, \ldots, M-1$, $\bar{a}_1 = 55$, $\bar{a}_2 = -59$, $\bar{a}_3 = 37$, $\bar{a}_4 = -9$, and

$$\theta^l = \begin{pmatrix} \left(\frac{1}{24}\sum_{j=0}^3 a_j h_1'((l-j)\Delta t) - \mathrm{d}h_1^{l-j}\right)\mathbf{z}^1 + \left(\frac{1}{24}\sum_{j=0}^3 a_j h_2'((l-j)\Delta t) - \mathrm{d}h_2^{l-j}\right)\mathbf{z}^2 \\ \left(\frac{1}{24}\sum_{j=0}^3 a_j v_1'((l-j)\Delta t) - \mathrm{d}v_1^{l-j}\right)\mathbf{z}^1 + \left(\frac{1}{24}\sum_{j=0}^3 a_j v_2'((l-j)\Delta t) - \mathrm{d}v_2^{l-j}\right)\mathbf{z}^2 \end{pmatrix},$$

where $a_0 = 9$, $a_1 = 19$, $a_2 = -5$, $a_3 = 1$. Assuming that $\Phi \in C^5(0, T_1 + 2\Delta t)^4$, where T_1 is as in Lemma 10, then $|\theta^l|$ and $|\bar{\theta}^l|$ can be bounded above by

$$\max\{|\theta^l|, |\bar{\theta}^l|\} \le c_4\Delta t^4 \sup_{t/\Delta t\in[l-6,l+2]}\{|\Phi^{(5)}(t)|\}.$$

Assume further that $\Phi(0) = \Phi'(0) = \cdots = \Phi^{(5)}(0) = \mathbf{0}$. Define $\Phi(t) = \mathbf{0}$ and $\mathbf{u} = \mathbf{0}$ for $t < 0$. Then $\mathbf{u} \in C^5((-\infty, T_1))$ and $(\mathrm{d}/\mathrm{d}t)\mathbf{u} = \mathbf{f}(t, \mathbf{u})$ for all $t \in (-\infty, T_1)$. Moreover

$$\max\{|\theta^l|, |\bar{\theta}^l|, l \le T_1/\Delta t\} \le c_4\Delta t^4 \sup_{t\in[0,T_1+2\Delta t]}\{|\Phi^{(5)}|\}.$$

Since the Lipschitz estimate on $\mathbf{f}$ is not a global estimate, Lemma 11 cannot be applied directly to the scheme (18). However, an argument similar to the one in Lemma 10 can be used to show that it is applicable to $\mathbf{f}$ over a

time interval $[0, T_2]$ where $T_2 \to T_1$ as $\Delta t \to 0$. Because we are interested in deriving a posteriori error estimates for $\mathbf{u}^l$, a different line of reasoning will be pursued.

Let $\tilde{T} \le T_1$, and set $\tilde{\sigma}(\tilde{T}) = \max\{|\mathbf{u}^l|, |\bar{\mathbf{u}}^l| : l \le \tilde{T}/\Delta t\}$. Note that $\tilde{\sigma}$ depends implicitly on Δt, Δx, and M, but we view these as fixed for now. In consequence, the quantity $\tilde{\sigma}$ is known, at least a posteriori. If we set

$$B(\tau) = \{\mathbf{v} \in \mathbb{R}^{2(m-1)} : |\mathbf{v}| \le \max\{\tilde{\sigma}(\tau), 1 + \sigma(\tau)\}\},$$

where $|\cdot|$ still connotes the l_∞-norm on $\mathbb{R}^{2(m-1)}$, then when $\tilde{T} \le T_1$, all the quantities $\mathbf{u}^l$, $\bar{\mathbf{u}}^l$ and $\mathbf{u}(t)$ belong to $B(\tilde{T})$ for $t, l\Delta t \in [0, \tilde{T}]$. In this situation, we replace $\mathbf{f}$ by a function $\tilde{\mathbf{f}}$ equal to $\mathbf{f}$ on $[0, \tilde{T}] \times B(\tilde{T})$, and such that $\tilde{\mathbf{f}}(t, \mathbf{y})$ is globally lipschitz continuous in $\mathbf{y}$ for $t \in [0, \tilde{T}]$ with a Lipschitz constant not exceeding that for $\mathbf{f}$ restricted to $B(\tilde{T})$. This is possible because the temporal-dependence and the $\mathbf{y}$-dependence of $\mathbf{f}$ are decoupled. In particular, a bound for the Lipschitz constant for $\mathbf{f}$ is

$$K(\tilde{T}) \equiv C_L(1 + 2\max\{\tilde{\sigma}(\tilde{T}), 1 + \sigma(\tilde{T})\}).$$

Since $\mathbf{u}^l$, $\bar{\mathbf{u}}^l$, for $t, l\Delta t \in [0, \tilde{T}]$, may be viewed equivalently as having been generated either by $\tilde{\mathbf{f}}$ or $\mathbf{f}$, Lemma 11 applies and yields

$$|\mathbf{u}^l - \mathbf{u}(l\Delta t)| \le c_5\left(1 + \frac{3}{8}K(\tilde{T})\Delta t\right)\Delta t^4\frac{e^{c_d\tilde{T}} - 1}{c_d}\left(\sup_{t\in[0,\tilde{T}]}|\mathbf{u}^{(5)}(t)| + \sup_{t\in[0,\tilde{T}+2\Delta t]}|\Phi^{(5)}(t)|\right)$$

for all $l \le \tilde{T}/\Delta t$, where $c_5 = \max\{c_3, c_4\}$ is a numerical constant and

$$c_d = c_d(\sigma(\tilde{T}), \tilde{\sigma}(\tilde{T})) = \tfrac{1}{12}K(\tilde{T}(17 + 30K(\tilde{T})\Delta t).$$

Combining this estimate with (21) and the bounds on $\mathbf{u}(t)$, one obtains for $0 \le \tilde{T} \le T_1$ and for all $l \le \tilde{T}/\Delta t$, that

$$\begin{aligned}|\mathbf{u}^l - \mathbf{U}(l\Delta t)| &\le |\mathbf{u}^l - \mathbf{u}(l\Delta t)| + |\mathbf{u}(l\Delta t) - \mathbf{U}(l\Delta t)| \\ &\le \psi(\tilde{T}) + c_5\left(1 + \frac{3}{8}K(\tilde{T})\Delta t\right)\Delta t^4\frac{e^{c_d\tilde{T}} - 1}{c_d} \\ &\quad\times\left(\sup_{t\in[0,\tilde{T}]}|\mathbf{u}^{(5)}| + \sup_{t\in[0,\tilde{T}+2\Delta t]}\{|\Phi^{(5)}(t)|\}\right) \equiv e_2(t),\end{aligned}$$

where, on account of the earlier estimates,

$$\begin{aligned}e_2(t) &= c_2\Delta x^4 Q_1(\sigma_i(t), 0 \le i \le 4)[e^{2C_L(1+\sigma_0(t))t} - 1]/(2C_L(1 + \sigma_0(t))) \\ &\quad + c_5\left(1 + \frac{3}{8}K(\tilde{T})\Delta t\right)\Delta t^4\frac{e^{c_d\tilde{T}} - 1}{c_d}\left[\sup_{t\in[0,\tilde{T}]}|\mathbf{u}^{(5)}(t)| + \sup_{t\in[0,\tilde{T}+2\Delta t]}\{|\Phi^{(5)}(t)|\}\right].\end{aligned}$$

Thus e_2 provides an upper bound for the total error in the fully discrete scheme. In particular, for fixed $\tilde{T} > 0$,

$$|u_i^l - U(i\Delta x, l\Delta t)| \le c_6(\Delta t^4 + \Delta x^4),$$

where c_6 is independent of Δt, Δx, and M, but depends on h_1, h_2, v_1, v_2, N, W, $\tilde{T}$, and $\tilde{\sigma}(\tilde{T})$.

Theorem 12. Let (N, W) be the solution to (4) and (5) with $f_1 = f_2 = 0$ and $\Phi = (h_1, h_2, v_1, v_2)$ belonging to $C^5(0, T)^4$, where $T > 0$ and $\Phi^{(i)}(0) = \mathbf{0}$, for $i = 0, 1, \ldots, 5$. Let M be a positive integer and $\Delta x = L/M$. Let Δt

be a positive parameter, and presume Δx, $\Delta t \leq 1$. Let $\mathbf{u}^l$ be the solution of (18), let $\tilde{T} \leq T_1$ be as defined in (19), and set

$$\tilde{\sigma}(T) = \max\{|\mathbf{u}^l|, |\bar{\mathbf{u}}^l|, l \leq T/\Delta t\}.$$

Then it follows that

$$\max\{|N(i\Delta x, l\Delta t) - n_i^l|, |W(i\Delta x, l\Delta t) - w_i^l|\} \leq c_6(\Delta t^4 + \Delta x^4)$$

for any i and l with $1 \leq i \leq M-1$ and $1 \leq l \leq \tilde{T}/\Delta t$, where c_6 is independent of Δt, Δx, M, but depends on h_1, h_2, v_1, v_2, N, W, $\tilde{T}$ and $\tilde{\sigma}(\tilde{T})$.

5. Numerical experiments

5.1. Convergence and efficiency tests

The convergence estimate $c(\Delta x^4 + \Delta t^4)$ for the scheme is checked numerically by using the exact travelling-wave solution

$$\begin{aligned} W(x,t) &= 3k\,\mathrm{sech}^2\frac{3}{\sqrt{10}}(x - kt - x_0), \quad k = \pm\frac{5}{2}, \\ N(x,t) &= \frac{15}{4}\left(-2 + \cosh\left(3\sqrt{\frac{2}{5}}(x - kt - x_0)\right)\right)\mathrm{sech}^4\left(\frac{3(x - kt - x_0)}{\sqrt{10}}\right), \end{aligned} \tag{22}$$

which was obtained by Chen [13]. We chose $x_0 = 20$ and $L = 40$ so that the crest of the wave is placed at the middle of the channel. The exact values of $N(x,0)$, $W(x,0)$, $N(0,t)$, $W(0,t)$, $N(L,t)$ and $W(L,t)$ are used for the initial- and boundary-conditions of N and W. All the numerical computations were performed on a DEC Alpha station.

The first test was designed to demonstrate that the error from the spatial discretization is of order Δx^4. This is accomplished by fixing the step size in the time direction and varying the step size in space. We took $\Delta t = 0.001$ and $\Delta x = 0.25/2^k$ for $k = 1, 2, 3, 4, 5, 6$, and compared the numerically generated approximation with the exact solution at $T = 1$ for each value of k. The max-norms of the errors in N and W, E_N^∞ and E_W^∞, respectively, were computed. The outcome is shown in Table 1.

The structure of Table 1 is as follows. The first column corresponds to the step size in space and the second column presents the CPU time used to obtain the numerical solution for each step size. Increasing k by 1 halves the step size which results in the number of mesh points being doubled. The ratio of CPU time used for step size

Table 1

k	CPU (s)	Ratio	E_N^∞	Ratio	E_W^∞	Ratio
1	2.71		0.1015		0.4193E−1	
2	5.33	1.97	0.7030E−2	14.4	0.2812E−2	14.9
3	10.73	2.10	0.4506E−3	15.6	0.1778E−3	15.8
4	21.90	2.04	0.2824E−4	16.0	0.114E−4	16.0
5	44.72	2.04	0.1766E−5	16.0	0.6965E−6	16.0
6	103.3	2.31	0.1089E−6	16.2	0.4297E−7	16.2

$L = 40$, $T = 1$, $\Delta t = 0.001$, $\Delta x = 0.25/2^k$.

Table 2

k	CPU (s)	Ratio	E_N^∞	Ratio	E_W^∞	Ratio
1	30.0		0.1707E−2		0.7658E−3	
2	60.3	2.01	0.1029E−3	16.6	0.4330E−4	17.7
3	122	2.02	0.6312E−5	16.3	0.2463E−5	17.6
4	246	2.02	0.3862E−6	16.3	0.1460E−7	16.9
5	497	2.02	0.2363E−7	16.3	0.8890E−8	16.4
6	984	1.98	0.1285E−8	18.4	0.5182E−9	17.2

$L = 40$, $T = 1.00$, $\Delta t = 0.0625/2^k$, $\Delta x = 2^{-10}$.

h_k and h_{k-1} is shown in column three. This ratio was seen to be about 2, thus confirming that the theoretical optimal-order efficiency of the scheme is attained. The fourth column shows the maximum absolute error at the mesh points between the exact solution N and the corresponding numerical approximation. The ratio of the error for step size h_{k-1} and h_k is shown in the fifth column. It appears that halving the step size in space results in the error being decreased by approximately 16 times, thereby demonstrating that the discretization error is of order Δx^4. Columns 6 and 7 are similar to columns 4 and 5, respectively, but for the variable W. Using the data for the CPU time for $k = 5$, one finds that the average CPU time used per point, per time step and per variable is approximately $0.448 \times 0.25/(40 \times 1000 \times 2^6) \approx 4.367\ \mu$s.

The second set of tests was organized to demonstrate that the error from the temporal integration is of order Δt^4. This was done by fixing the step size in the spatial discretization and varying the temporal step size. The spatial discretization was fixed at 2^{-10}, a value sufficiently small that the error derived thereform is negligible compared to that generated by the temporal discretization. The time step Δt was taken to be $\Delta t = 0.0625/2^k$ for $k = 1, 2, 3, 4, 5, 6$, and the numerically generated approximation was compared with the exact solution at $T = 1$ for each k. The max-norms of the error associated with N and W, E_N^∞ and E_W^∞, were computed and are shown in Table 2. The structure of Table 2 is similar to Table 1. Column 2 shows the optimal efficiency obtained and columns 5 and 7 indicate that the discretization error in time is of order Δt^4.

Tables 1 and 2 are consistent with the unconditional stability of the scheme since the numerical approximation is bounded over quite large variations in the ratio of Δt to Δx. It is worth noting that the numerical experiments indicate that for fixed Δx and Δt, the overall error grows linearly in t.

5.2. *Generation of clean solitary waves*

To numerically simulate the collision of solitary waves, one needs to have in hand accurate or "clean" numerical approximations of these solitary waves. Generating a clean solitary wave in a laboratory environment is a rather difficult task. In contrast, we will show that generating clean solitary-wave solutions numerically is not difficult, even when exact solutions are not available, which is the case for this system (the exact solution (22) is not a solitary-wave solution because N changes sings). The procedure for numerically generating a solitary wave may be described heuristically as letting a wave that is close to a solitary wave evolve in an extensive water channel for a relatively long time. After the leading solitary wave separates from the rest of the disturbance, we may cut it off from the remainder and have, to a very good approximation, a clean solitary-wave solution. Numerically, this was accomplished by commencing with initial data that resembles a solitary wave and letting it evolve for a certain time according to a numerical simulation of the evolution equation via the scheme outlined above. When the principal elevation has shaken off a dispersive tail, and often, smaller solitary waves, it is isolated numerically by setting the remainder of the signal to zero. It is then pulled back to the left-hand side of the spatial interval of integration and the process repeated. A few interations of this procedure were needed to produce an accurate solitary traveling wave.

In practice, we started the numerical simulation with zero initial conditions and let a single "solitary" wave, which was a lower-order aproximation to the actual solitary wave, enter via the boundary conditions from the left side of the spatial domain.

To find a suitable approximate solitary-wave solution, it is convenient to introduce a system which explicitly expresses the order of magnitude for all the terms appearing in (3). Using the dimensionless variables,

$$x = \lambda\tilde{x}, \quad t = \lambda\tilde{t}/c_0, \quad \eta = a\tilde{\eta}, \quad w = ga\tilde{w}/c_0, \tag{23}$$

and letting $\alpha = a/h$ and $\beta = h^2/\lambda^2$ be the small parameters corresponding to nonlinear and dispersive effects, respectively, the system (3) becomes

$$\begin{aligned} &\tilde{\eta}_{\tilde{t}} - \tfrac{1}{6}\beta\tilde{\eta}_{\tilde{x}\tilde{x}\tilde{t}} = -\tilde{w}_{\tilde{x}} - \alpha(\tilde{\eta}\tilde{w})\tilde{x}, \\ &\tilde{w}_{\tilde{t}} - \tfrac{1}{6}\beta\tilde{w}_{\tilde{x}\tilde{x}\tilde{t}} = -\tilde{\eta}_{\tilde{x}} - \alpha\tilde{w}\tilde{w}_{\tilde{x}}. \end{aligned} \tag{24}$$

If $\alpha = \beta = 0$ in (24) and attention is restricted to solutions moving to the right, it is found upon solving the linear wave equation that $\tilde{w} = \tilde{\eta}$. To correct for the small but non-zero effects of nonlinearity and dispersion, it is a standard procedure to suppose that

$$\tilde{w} = \tilde{\eta} + \alpha A + \beta B,$$

where A and B are functions of $\tilde{\eta}$, $\tilde{x}$ and $\tilde{t}$ (cf. [27]). Substituting this expression for $\tilde{w}$ into (24), one obtains the pair of equations

$$\begin{aligned} &\tilde{\eta}_{\tilde{t}} - \tfrac{1}{6}\beta\tilde{\eta}_{\tilde{x}\tilde{x}\tilde{t}} = -\tilde{\eta}_{\tilde{x}} - \alpha A_{\tilde{x}} - \beta B_{\tilde{x}} - \alpha(\tilde{\eta}^2)_{\tilde{x}}, \\ &\tilde{\eta}_{\tilde{t}} - \tfrac{1}{6}\beta\tilde{\eta}_{\tilde{x}\tilde{x}\tilde{t}} = -\tilde{\eta}_{\tilde{x}} - \alpha A_{\tilde{t}} - \beta B_{\tilde{t}} - \alpha\tilde{\eta}\tilde{\eta}_{\tilde{x}}, \end{aligned} \tag{25}$$

after neglecting the higher-order terms. Since these two equations have to be consistent, and using the lowest-order relation $\partial_x = \partial_t + O(\alpha, \beta)$ on the terms linear in α and β, we find

$$2\alpha A_{\tilde{x}} + 2\beta B_{\tilde{x}} - \alpha\tilde{\eta}\tilde{\eta}_{\tilde{x}} + \alpha(\tilde{\eta}^2)_{\tilde{x}} = 0,$$

which yields

$$A = -\tilde{\eta}^2/4, \quad B = 0.$$

Substituting this relation into either of the equations in (25) and solving for $\tilde{\eta}$, we obtain the first-order approximation to a traveling-wave solution, namely

$$\begin{aligned} &\tilde{\eta} = \tilde{\eta}_0 \operatorname{sech}^2\left(\frac{1}{2}\sqrt{\frac{3\alpha\tilde{\eta}_0}{\beta k}}(\tilde{x} - k\tilde{t} - \tilde{x}_0)\right) \quad \text{with } k = 1 + \tfrac{1}{2}\alpha\tilde{\eta}_0, \\ &\tilde{w} = \tilde{\eta} - \tfrac{1}{4}\alpha\tilde{\eta}^2. \end{aligned}$$

Rewrite this appeoximate solution in the non-dimensional variables N, W, $\hat{x}$, $\hat{t}$ to obtain

$$\begin{aligned} &N(\hat{x}, \hat{t}) = N_0 \operatorname{sech}^2\left(\frac{1}{2}\sqrt{\frac{3N_0}{\hat{k}}}(\hat{x} - \hat{k}\hat{t} - \hat{x}_0)\right) \quad \text{with } \hat{k} = 1 + \tfrac{1}{2}N_0, \\ &W(\hat{x}, \hat{t}) = N - \tfrac{1}{4}N^2, \end{aligned} \tag{26}$$

which we view as an approximation to a solitary-wave solution of the system (4). This approximation is familiar from the unidirectional Korteweg–de Vries theory.

Table 3
Solitary-wave height versus phase velocity

N_0	N_s	$c/\sqrt{gh}$	N_0	N_s	$c/\sqrt{gh}$
0.1	0.0995	1.0488	0.9	0.8109	1.3578
0.2	0.1975	1.0953	1.0	0.8847	1.3868
0.3	0.2936	1.1395	1.2	1.0201	1.4385
0.4	0.3875	1.1815	1.4	1.1384	1.4825
0.5	0.4787	1.2211	1.6	1.2393	1.5193
0.6	0.5669	1.2586	1.8	1.3226	1.5490
0.7	0.6518	1.2938	2.0	1.3885	1.5722
0.8	0.7332	1.3269	2.5	1.4804	1.6040

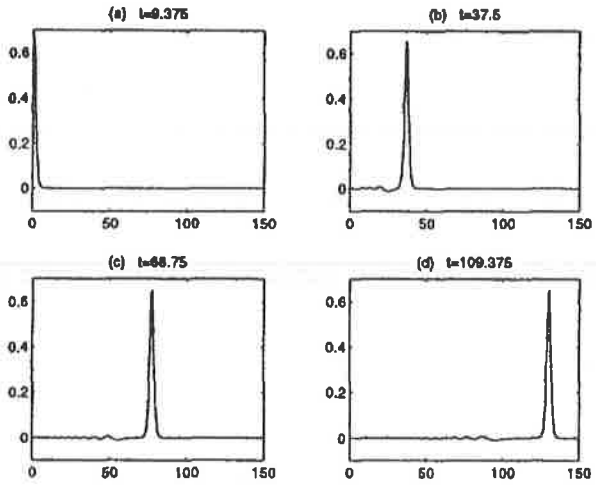

Fig. 1. A solitary wave followed by a dispersive tail.

The formulas in (26) are used to generate clean solitary-wave solutions numerically. In the numerical computation, we choose $L = 150$, $\Delta x = \Delta t = 1/64$, $x_0 = 12$ for $N_0 > 0.4$ and $x_0 = 18$ for $N_0 \leq 0.4$, so that the compatibility condition at $\hat{x} = 0, \hat{t} = 0$ was satisfied to within the tolerance 3×10^{-5}. To generate different size solitary waves, we let N_0 range between 0.1 and 2.5, which resulted in solitary waves with height N_s between 0.0995 and 1.4800 (see Table 3). Solitary waves higher than 1.4800 can also be generated by using $W(\hat{x}, \hat{t}) = N(\hat{x}, \hat{t})$ where $N(\hat{x}, \hat{t})$ is as in (26) and using larger N_0. Of course no physical relevance should be imputed to solitary-wave solutions of larger amplitude since as a model of physical reality, the system (4) subsists in part on a small-amplitude assumption. Indeed for the full Euler equations, it is well known that there are no solitary-wave solutions beyond the so-called wave of the greatest height (cf. [1]). However, the large-amplitude solutions provide a good test of the computer code implementing the algorithm described in Section 3.

The time evolution of the solution for $N_0 = 0.7$ (which generates a solitary-wave solution of height 0.6518) is shown in Figs. 1(a)–(d), where a solitary wave develops, followed by a dispersive tail. In the approximate solution at $\hat{t} = 109.375$ (see Fig. 1(d)) has its dispersive tail cut out by shifting the solution to the left by a distance 115.625 and filling the right with zero, one obtains a relatively clean solitary-wave solution in the interval $[0, L]$. The resulting approximate solution can be further filtered by using it as initial data and letting it evolve, again clipping the dispersive tail that emerges. To have the relative magnitude of the tail that emerges, N_{tail}/N_s, smaller than 3.5×10^{-6}, we used one filtering step for $N_0 \geq 0.8$, two filtering steps for $N_0 = 0.5, 0.6, 0.7$, three filtering steps for $N_0 = 0.3, 0.4$ and four filtering steps for $N_0 = 0.2$. In the case $N_0 = 0.1$, the relative magnitude of the

Table 4(a)
$\max(N_{\text{tra}} - N)/N_s$

N_s	$t = 20$	$t = 40$	$t = 60$	$t = 80$
0.0995	1.526(−4)	2.003(−4)	2.152(−4)	2.256(−4)
0.2936	6.720(−4)	8.1574(−4)	1.223(−3)	1.631(−3)
0.4787	3.654(−4)	7.309(−4)	1.096(−3)	1.462(−3)
0.6518	1.438(−4)	2.8755(−4)	4.316(−4)	5.700(−4)

Table 4(b)
Size of the tail

N_s	0.0995	0.1975	0.2936	0.3875	0.4787	0.5669	0.6518	0.7332
N_{tail}/N_s	2.2(−4)	3.5(−6)	1.6(−6)	2.1(−8)	3.7(−7)	4.5(−9)	4.0(−9)	5.8(−9)

dispersive tail is 2.2×10^{-4} with five filtering steps. The magnitude of the tail is recorded in Table 4(b). Smaller values of L can save computational cost and memory, but require more filtering steps.

Outcomes entirely similar to that depicted in Fig. 1 are found for N_0 ranging from 0.1 to 2.5. For each N_0, the normalized phase velocity $c/\sqrt{gh}$ and the height N_s of the resulting solitary wave are computed and listed in Table 3. These data have been checked by halving the spatial and temporal discretization and by doubling the length of the wave tank. For $N_0 = 0.5$, which generates an approximate solitary-wave solution with $N_s = 0.4786563$ and $c/\sqrt{gh} = 1.2211242$, the change in N_s and c is less than 1.5×10^{-6} and 8.7×10^{-6}, respectively, when the result is compared with that obtained by doubling the number of mesh points. To further ascertain how near to a solitary wave we arrived by the process of filtering the approximate profile in (26), another experiment was conducted. The free surfaces and velocity profiles of some of our "clean" solitary waves were taken again as initial data for the discrete analog (18) of (4), located so that the boundary conditions are sensibly zero. We then compared the evolution of these data under the auspices of (18) with the initial data translated at what we recorded in Table 3 to be its phase velocity. (The latter quantity is denoted N_{tra} in Table 4 below.) The maximum norms of the differences between the two just-mentioned versions of the free surface, E_N^∞, as a function of t are recorded in Table 4(a) (which is scaled by N_s). The maximum value of the difference occurs near the crest of the wave for all displayed values of N_s except $N_s = 0.0995$. The differences with regard to W and the L_2-norms of the differences behave exactly like E_N^∞, and they all comprise less than 0.1% of the mass or momentum in the waves. In Table 4(b), the magnitude of the dispersive tail N_{tail}, scaled by N_s, is recorded. Tables 4(a) and (b) provide further evidence that the waves we generated are indeed very nearly solitary waves which travel with the speed noted in Table 3. Even with five filtering steps, $N_0 = 0.0995$ was apparently the least exact of the approximate solitary waves reported here.

The data in Table 3 record approximately the relationship between maximum wave height and phase speed for solitary waves. According to the convergence study in which the spatial and temporal meshes were halved and the comparisons displayed in Table 4, we have considerable confidence in at least the first three decimals in Table 3. In consequence, the relationship between wave height and phase speed for solitary-wave solutions can sensibly be compared with theoretical results obtained from the Euler equations and with existing experimental data. This comparison is helpful in determining the range over which the model system (4) might be a useful approximation to reality.

The theoretical result we compare with is the systematic expansion of the phase velocity with respect to the height of the solitary-wave solution of the Euler equations for the flow of a perfect fluid, namely

$$c = (gh)^{1/2}(1 + \tfrac{1}{2}N_s - \tfrac{3}{20}(N_s)^2 + \tfrac{3}{56}(N_s)^3 + \cdots) \tag{27}$$

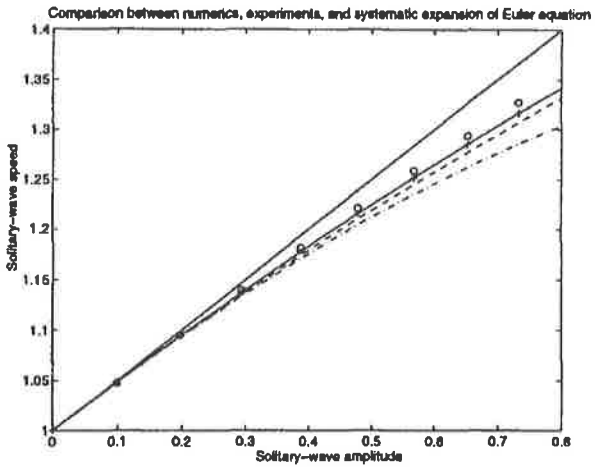

Fig. 2. Comparison between (27), (28) and numerical simulation of (4): (o) numerical data using (4); (− + −) experimental prediction (28); — two terms of (27); (−·) three terms of (27); (− −) four terms of (27).

(cf. [17,25]; the convergence of this expansion has not been proven). The explicit solitary wave solutions to unidirectional models, for example the KdV equation and the regularized long-wave equation (see [2]), have phase velocities which are the first-order approximation of (27),

$$c = (gh)^{1/2}(1 + \tfrac{1}{2}N_s).$$

On the other hand, Scott Russell's experimental results were accurately mirrored by the presumption

$$c = (gh)^{1/2}\sqrt{1 + N_s} \tag{28}$$

(Russell [24]). In Fig. 2, we compare our numerically generated data ('o' points) with (28) ('− + −' line) and the first-order ('—' line), second-order ('−·' line) and third-order ('− −' line) approximation of (27). The graph shows that the numerical results using the model (4) are close to the prediction made on the basis of experiments and to the third-order approximation of (27) for a wide range of solitary-wave heights.

The data in Table 3 that are displayed in Fig. 2 are instructively used to fit a Taylor polynomial. That is, suppose the solitary-wave solutions approximated in Table 3 belong to a continuous branch of solution (see [6]) such that the phase speed c is an analytic function of the maximum amplitude N_s, say with Taylor expansion about the origin of the form

$$c = f(N_s) = a_0 + a_1 N_s + a_2 N_s^2 + \cdots. \tag{29}$$

If we consider k entries (c_i, N_i), $1 \le i \le k$, in Table 3 starting with the smallest value of $N = N_s$, then it is elementary to obtain an approximate Taylor polynomial of degree $k-1$ that passes exactly through these k points. That is, if f_k is the truncation of f so that

$$f_k(N) = \tilde{a}_0 + \tilde{a}_1 N + \cdots + \tilde{a}_{k-1} N^{k-1},$$

then f_k is uniquely determined by the equations

$$c_i = f_k(N_i), \quad 1 \le i \le k. \tag{30}$$

Using the first three points, it is found that

$$f_3(N) = 1.0001 + 0.4968N - 0.0750N^2,$$

while the use of the first four or five points gives

$$f_4(N) = 0.9999 + 0.4999N - 0.0922N^2 + 0.0291N^3,$$

and

$$f_5(N) = 0.9997 + 0.5053N - 0.1306N^2 + 0.1411N^3 - 0.1145N^4.$$

Comparing these polynomials with the formal expansion (27) and Scott Russell's formula (28), it is evident that the first two terms were captured rather well, despite the fact that the values of N used to obtain them are neither small, nor especially close together.

5.3. *Head-on collision of solitary waves of equal sizes*

An interesting numerical experiment to be discussed now is comprised of a pair of solitary waves of equal height, but propagating in the opposite direction, interacting in a head-on collision. As is well-known, this interaction is equivalent to the ideal reflection of a solitary wave on a vertical wall, a fluid motion that has some practical interest as a crude approximation to what happens when a train of long waves reflects off a coast line. The head-on collision of two equal-sized solitary waves is classified as wave–wave weak interaction in [21] because the interaction time is very short when compared with that of two solitary waves interacting as they travel in the same direction. Our numerical results will be compared with existing theoretical and numerical results obtained from the Euler equations and with experimental outcomes.

The numerical computations are initiated using the clean solitary waves generated as previously described. Two equal-sized solitary waves moving in opposite directions are set in motion by letting

$$N_{\text{new}}(\hat{x}) = \begin{cases} N(\hat{x}), & 0 \le \hat{x} \le \frac{1}{2}L, \\ N(L-\hat{x}), & \frac{1}{2}L \le \hat{x} \le L, \end{cases}$$

$$W_{\text{new}}(\hat{x}) = \begin{cases} W(\hat{x}), & 0 \le \hat{x} \le \frac{1}{2}L, \\ -W(L-\hat{x}), & \frac{1}{2}L \le \hat{x} \le L, \end{cases}$$

where (N, W) is a clean, right-moving, solitary-wave solution of (4) whose elevation is placed near the left-hand end of the spatial domain. For the integration of (4) with these initial data, Δx, Δt and L are chosen as before, namely $\Delta x = \Delta t = 0.5/32$ and $L = 150$.

Fig. 3 shows a typical time evolution of the head-on collision of two equal-sized solitary waves with the amplitude to water depth ratio $N_s = 0.4787$. From (a) to (b), the solitary waves traveled for a time period $\hat{t} = 23.42$ with essentially no change of shape or amplitude. Part (c) shows the interaction of the two waves; notice that the maximum wave height at interaction is 1.0504, which is substantially more than double the incident wave height. Fig. 3(d) is taken after the interaction when the two waves are moving away from each other. In (e), the two solitary waves are further apart and are seen to be quite similar to those in (a). A closer look at the interval between the separating solitary waves in (d) and (e) shows that there has been generated a secondary dispersive wave of extremely small magnitude. As is usual for purely dispersive waves, it spreads and its amplitude diminishes with time.

Figs. 4 and 5 provide a more detailed view of the interaction. Fig. 4 shows the numerical approximation immediately after the interaction at $\hat{t} = 54.88$; the genesis of the dispersive train is clearly evident. The dispersive tail has at this time an amplitude of 0.000372 (scaled by h) which is about 0.077% of the incident wave height. The presence of the dispersive disturbance indicates that the interaction is not "exact", so these traveling waves are not solitons.

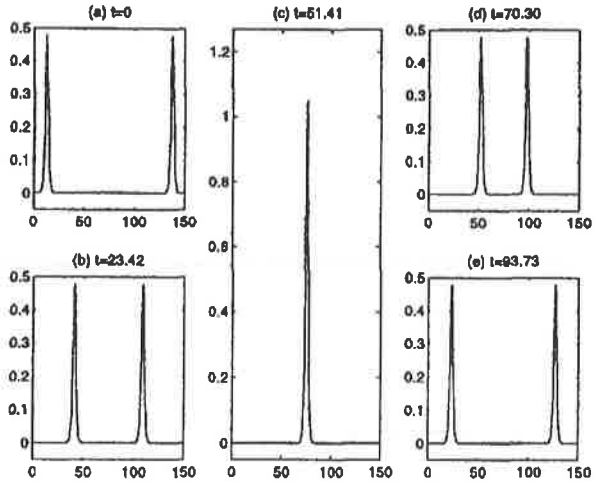

Fig. 3. Time evolution of a head-on collision.

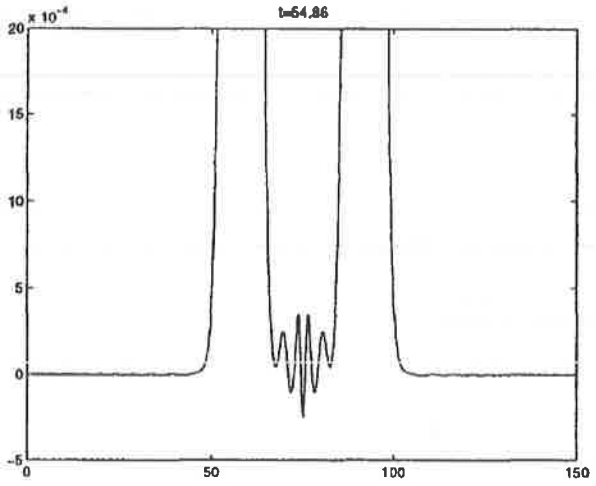

Fig. 4. Dispersive tail.

In Fig. 5, we study carefully the solitary-wave amplitude before and after the interaction. The maximum value of the wave is plotted against time in Fig. 5(a) and magnified at the vertical axis between 0.4785 and 0.4790 in Fig. 5(b). Before the interaction ($\hat{t}$ ranging between 0 and 34), the two solitary waves are moving towards each other with no change of amplitude. Between about $\hat{t} = 34$ and $\hat{t} = 60$, the two solitary waves interact in a head-on collision and the amplitude jumped to 1.050449 at $\hat{t} = 40.78$, which is more than double the incident wave height (cf. Fig. 5(a)). After the interaction ($\hat{t}$ ranging between 60 and 80), two elevations emerged and moved away from each other. These appear to settle down to solitary waves with amplitudes slightly smaller than those of the incident waves. The loss in mass and momentum is reflected in the generation of the dispersive train. One observes in Fig. 5(b) that after the interaction, the amplitude of the waves emerging from the interaction reaches a minimum and then recovers to very nearly the height before the interaction. The permanent loss of amplitude, which went into the dispersive tail, is very small. The reduced height immediately after the interaction is transitional. Notice that if the temporal integration is not carried far enough, one would observe a larger loss of magnitude because the solution would still be in this transitional phase.

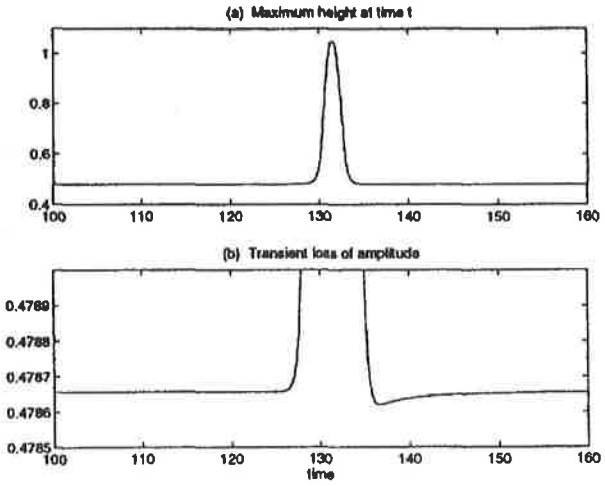

Fig. 5. Wave amplitude against time.

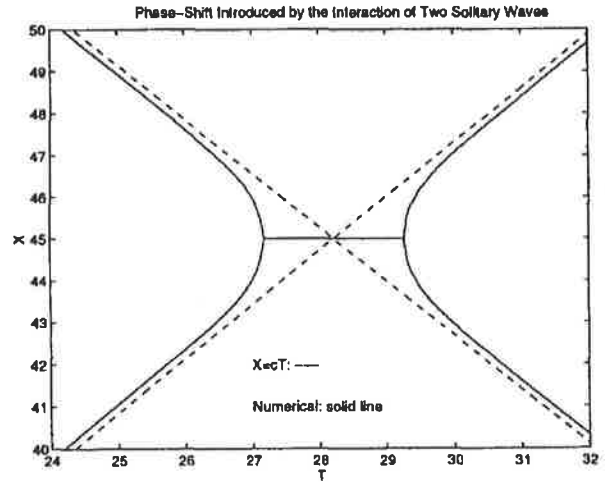

Fig. 6. A typical phase-shift diagram.

The amplitude of the wave at the interaction being more than double the incident wave height is a typical feature of a nonlinear interaction. Another feature of the nonlinearity of the interaction is the phase shift. This is the property often exhibited by interacting solitary waves having their center of mass translated in a way not described by movement at constant speed. A typical phase-shift diagram is presented in Fig. 6 ($N_s = 0.6518$), in which the location of the two peaks is plotted against time $\hat{t}$. It is clear from Fig. 6 that the solitary waves are shifted back (delayed) due to the interaction.

Results similar to those just described are found for computations conducted with N_s ranging between 0.0995 and 0.8847. The outcome of a series of such numerical experiments is summarized in Table 5. The incoming solitary-wave amplitudes N_s are recorded in column 1. The maximum amplitude run-up at the peak of the interaction N_{max} is shown in column 2. The gain of the maximum run-up when compared with twice the incident wave amplitude $(N_{max}/2N_s) - 1$ comprises column 3. The phase shifts c_{shift} are written in column 4, which are the amounts of time the wave was delayed due to the interactions. The transient loss of amplitude $|N_s - N_{min}|/N_s$ is displayed in column 5, where N_{min} is the minimum wave amplitude following the interaction while the maximum excursion

Table 5
Head-on collision of two identical solitary waves

N_s	N_{max}	$(N_{max}/2N_s) - 1$	c_{shift}	$(N_s - N_{min})/N_s$	N_{disp}
0.0995	0.2037	0.0235	−0.1753	2.36(−4)	1.83(−5)
0.1975	0.4128	0.0450	−0.2460	2.34(−5)	1.1(−5)
0.2936	0.6250	0.0643	−0.2978	3.97(−5)	5.01(−5)
0.3875	0.8382	0.0816	−0.3382	6.24(−5)	1.88(−4)
0.4787	1.0505	0.0973	−0.3684	8.47(−5)	3.72(−5)
0.5669	1.2601	0.111	−0.3971	2.12(−4)	6.33(−4)
0.6518	1.4656	0.124	−0.4203	1.35(−4)	9.60(−4)
0.7332	0.6656	0.135	−0.4406	1.49(−4)	1.34(−3)
0.8109	0.146	0.146	−0.4585	1.76(−4)	1.77(−3)
0.8847	2.0450	0.156	−0.4730	1.97(−4)	2.22(−3)

of the dispersive tail after the interaction is recorded in column 6. It is seen from columns 2 and 3 that N_{max} and N_{max}/N_s are increasing with N_s. For N_s ranging between 0 and 0.7332, $(N_{max}/2N_s) - 1$ varies from 0 to 0.135, which means the maximum run-up at the middle is between 0% and 13.5% more than double the incident wave height. The data are consistent with the proposition that $(N_{max}/2N_s) - 1 \to 0$ as $N_s \to 0$, so going over to the linear theory in the limit of infinitesimal amplitude. The phase shift in column 4 also increases as N_s increases and likewise points to the property $c_{shift} \to 0$ when $N_s \to 0$. Column 5 confirms that for this model system, there is a transitional loss of magnitude, which is small when compared with the existing experimental results. It was noticed during the computations that the magnitude of this transitional loss and the height of the dispersive tail (column 6) are sensitive to the cleanness of the incoming solitary wave. One observes much larger secondary excursions due to the tails of the incoming disturbance when the initial configuration is not quite so close to a true solitary wave. If we use one, instead of four, filtering step for $N_0 = 0.2$, and then interact the resulting approximate solitary wave with itself in a head-on collision, the entries corresponding to row 2 in Table 5 are as follows.

N_s	N_{max}	$(N_{max}/2N_s) - 1$	c_{shift}	$(N_s - N_{min})/N_s$	N_{disp}
0.1975	0.4128	0.0450	−0.2460	1.7(−3)	5.8(−4)

Thus the noisier approximation generates considerably larger values of the transitional loss of magnitude and the maximum excursion of the dispersive tail.

The relative magnitude of this transitional loss of amplitude and the height of the dispersive wave both increase as N_s increases. (The values associated with $N_s = 0.0995$ may not be accurate because the incident solitary waves are not especially clean.) In our computations, we did not observe large permanent loss of amplitude. The solitary waves appear to always recover from their transitional loss and return to very nearly their original height. These observations are at odds with the experimental results of Renouard et al. [23]. The discrepancy between experimental outcomes and our numerical simulations owes to at least two major aspects. First, dissipative effects are always substantial in wave tanks on laboratory scales (cf. [4]). Second, it is quite difficult to generate a truly clean solitary wave in a laboratory setting. As just indicated, numerical simulations with less accurate approximations to solitary waves led to significant permanent loss of amplitude due to interaction, just as observed in the laboratory.

A quantitative comparison is now undertaken between numerical data in Table 5 and existing theoretical and numerical results obtained via the Euler equations, and with existing experimental results. We first compare the maximum height of the wave during interaction and the phase shift after the collision. Since the collision of equal-sized solitary waves is equivalent to the reflection of a solitary wave against a vertical wall in the absence of viscous effects, comparisons of the numerical simulations reported above can be made with theoretical and other results for

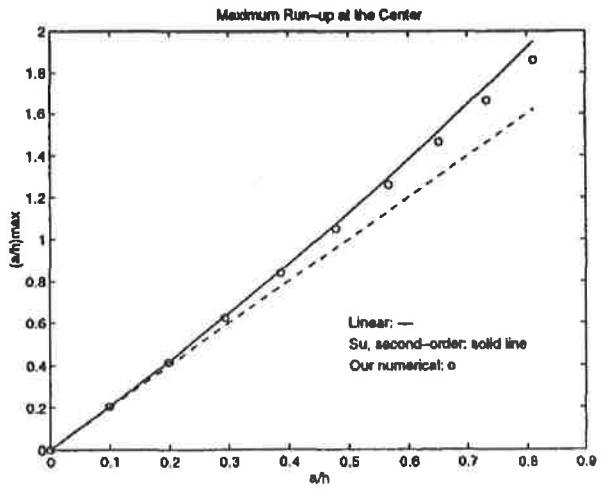

Fig. 7. Maximum run-up, interaction of two equal solitary waves: 'o' Numerical simulation using (8); (– –) one term of (31); (—) two terms of (31).

this latter problem. From the Euler equations, one obtains a systematic expansion of the maximum wave amplitude $N_{\max}$ along the wall in tems of N_s, which is (cf. [9,22,25])

$$N_{\max} = 2N_s + \tfrac{1}{2}(N_s)^2 + \tfrac{3}{4}(N_s)^3 + \cdots \tag{31}$$

and similarly for the phase-shift c_{shift}

$$\frac{c_{\text{shift}}}{h} = (N_s/3)^{1/2}(1 + \tfrac{7}{8}N_s + \cdots) \tag{32}$$

(the convergence of these series is again an open question, even for small values of N_s).

In Fig. 7, the maximum wave height at the center of the interaction is compared with both the first- and second-order approximations in (31). The numerical simulations agree with the second-order approximation more closely for a wide range of incident wave heights. The third-order approximation is more accurate only when N_s is sufficiently small.

If the numerically generated data in Table 5 are used to fit a cubic polynomial in the same way as indicated in (29) and (30), it is found that

$$N_{\max} \approx 1.9993N_s + 0.4967N_s^2 - 0.1916N_s^3 + \cdots$$

The phase shift introduced by the iteraction of the two solitary waves is shown in Fig. 8 along with the associated graph of the leading-order approximation (32) to the phase shift according to the Euler equations. The numerically generated values lie close to, but below those predicted by (32). One possible reason for the slight discrepancy is that we did not wait long enough in our computations for the outgoing waves to recover, and a small error in the phase speed could result in a relatively large error in C_{shift}.

Again using the numerically generated data to fit an approximation to a putative Talor expansion, one obtains

$$\frac{C_{\text{shift}}}{h} \approx (N_s/3)^{1/2}(0.9632 + 0.0106N_s - 0.1663N_s^2 + \cdots),$$

which has a leading term agreeing reasonably well with that in (32).

Overall, our numerically generated data show the system (4) models well solitary-wave propagation and interaction even when the amplitude of the wave is not especially small. Indeed, our numerical methods could handle amplitudes N_s at least as high as 7, which is of course not relevant to practical situations.

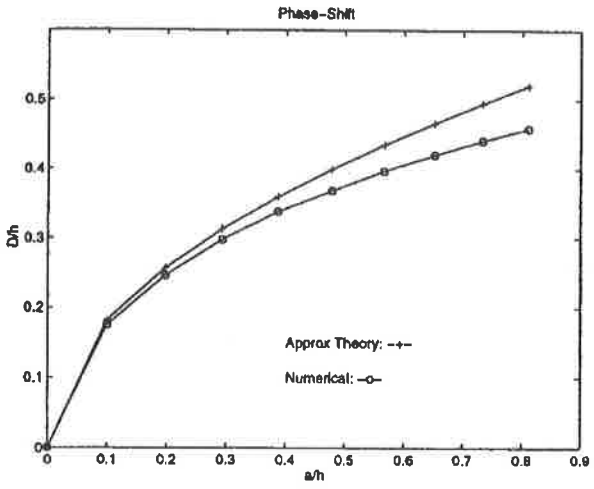

Fig. 8. Phase shift.

Comparison is now made between the numerical data and existing experimental results found in [11,20], and in particular with more recent results obtained in [23]. Regarding the reflection of a solitary wave from a plane vertical wall, the maximum run-ups on the wall in all the experiments agree pretty well with (31) and the phase shifts reported in [23] agree with (32) qualitatively and to some extent quantitatively. Reasons for the lack of detailed agreement with experiments certainly include the viscous effects in the boundary layer along the channel walls, which is not modeled here. Indeed, the comparisons of experimental data taken in a flume with the predictions of a unidirectional model related to (4) in [4] show clearly that detailed agreement at least for laboratory scales depends on accurate modeling of dissipative effects. In addition, the solitary waves generated in the laboratory are not clean, so the incident wave is not clean and the reflected wave encounters a dispersive tail as it comes off the wall. This aspect also was essentially absent in the numerical simulations. In [23], they also reported the transitional loss of magnitude and dispersive tails after the interaction, but with much larger magnitude than observed in our numerical computations. They found that $(N_s - N_{out})/N_s$ and N_{disp} depend on N_s at third-order. The magnitude of either the loss of amplitude or the dispersive tail is about 10% of the incident amplitude when N_s is about 0.6. As mentioned previously some of this discrepancy might come from the effect of the dispersive tails following the incident waves and the absence of a model for dissipative effects. Especially dissipative effects together with the process of generation mean that the waveform encountering the vertical wall may differ from that of a solitary wave. Because of the nature of our model system, which is only formally first-order correct with respect to the small parameter ϵ, we are not in a position to say if the change of amplitude is fifth-order in ϵ (see [10]) or third-order in ϵ (see [25]). We are currently working on higher-order Boussinesq systems for two-way propagation of water waves [14] and expect in due course to better understand these phenomena. We are also preparing our own experiments in which we will observe directly the collision of solitary waves rather than as modeled by interaction with a vertical wall.

Numerical experiments of head-on collisions have been reported in various papers. A modified Marker and Cell technique (SUMMAC) was used on the full Euler equations in [12,26], while Fourier methods were used in [18] on the Euler equations. In [25], the authors computed solutions using a Boussinesq-like system. Qualitatively, (31) and (32) agreed with all these numerical results. The major difference is the existence and the magnitude of permanent loss (the heights of the outgoing solitary waves are lower than that of the associated incoming solitary waves), the transitional loss and the dispersive tail. We concluded from our numerical results that there is a dispersive tail and a transitional loss of magnitude associated with the interaction, but the incoming and outgoing solitary waves

eventually have essentially the same height, the difference being less than 10^{-6}, a value which could not be observed in experiments.

5.4. Head-on collision of waves with different heights

Our third set of numerical experiments pertain to the head-on collision of different-sized solitary waves. The systematic expansion derived in [25] for the run-up at the height of the interaction is

$$N_{\max} = N_{\mathrm{R}} + N_{\mathrm{L}} + \tfrac{1}{2} N_{\mathrm{R}} N_{\mathrm{L}} + \cdots, \tag{33}$$

where N_{R} and N_{L} are the wave heights of the right- and left-moving solitary waves, respectively. The phase shifts for the right- and left-going waves are

$$\frac{C^{\mathrm{R}}_{\mathrm{shift}}}{h} = \left(\frac{N_{\mathrm{L}}}{3}\right)^{1/2} \left(1 + \frac{1}{8} N_{\mathrm{L}} + \frac{3}{4} N_{\mathrm{R}} + \cdots\right)$$

and

$$\frac{C^{\mathrm{L}}_{\mathrm{shift}}}{h} = -\left(\frac{N_{\mathrm{R}}}{3}\right)^{1/2} \left(1 + \frac{1}{8} N_{\mathrm{R}} + \frac{3}{4} N_{\mathrm{L}} + \cdots\right), \tag{34}$$

respectively.

It was observed in our numerical experiments that after the interaction, the higher wave first lost amplitude and then very nearly recovered its original height and the lower wave first gained height and then decreased almost to its original elevation. After this transition period, the two waves moved away from each other at almost the same heights they possessed before the interaction. Should the intergration be terminated too early, one might conclude that there is a considerable mass transfer from the higher wave to the lower wave. Both waves were shifted back (delayed) and there was a small dispersive wave between them after the interaction. For a series of wave heights of the right- and left-moving waves, we computed the maximum wave amplitudes at the interaction. These are listed in Table 6, while the phase shifts for the left-going waves are listed in Table 7. The phase shifts of the right-going waves can be found by switching the positions of the left- and right-going waves.

In Figs. 9 and 10, we compare the theoretical results in (33) and (34) by fixing the height of the left-going wave at $N_{\mathrm{L}} = 0.4787$, and letting the height of the right-going wave vary. Our numerical results accurately agree with (33) and with the leading term of (34).

Table 6
Run-up in head-on collision of different-sized waves

N_{L}	N_{R}							
	0.0995	0.1975	0.2936	0.3875	0.4787	0.5669	0.6518	0.7332
0.0995	0.2037							
0.1975	0.3060	0.4128						
0.2936	0.4064	0.5170	0.6250					
0.3875	0.5042	0.6185	0.7300	0.8382				
0.4787	0.5990	0.7169	0.8316	0.9429	1.0505			
0.5669	0.6907	0.8118	0.9296	1.044	1.1540	1.260		
0.6518	0.7788	0.9030	1.0236	1.1405	1.2533	1.3620	1.4656	
0.7332	0.8632	0.9902	1.1136	1.2329	1.3481	1.4590	1.5646	1.6656

Table 7
Phase shifts of the left-going wave

N_L	N_R							
	0.0995	0.1975	0.2936	0.3875	0.4787	0.5669	0.6518	0.7332
0.0995	0.1753	0.2538	0.3120	0.3570	0.3960	0.4318	0.4595	0.4925
0.1975	0.1782	0.2460	0.3024	0.3531	0.3854	0.4246	0.4546	0.4741
0.2936	0.1782	0.2436	0.2978	0.3403	0.3809	0.4145	0.4439	0.4694
0.3875	0.1714	0.2400	0.2943	0.3382	0.3738	0.4066	0.4399	0.4641
0.4787	0.1655	0.2366	0.2893	0.3337	0.3684	0.4001	0.4323	0.4561
0.5669	0.1627	0.2315	0.2849	0.3285	0.3637	0.3971	0.4234	0.4527
0.6518	0.1648	0.2248	0.2819	0.3226	0.3597	0.3942	0.4203	0.4426
0.7332	0.1590	0.2288	0.2800	0.3183	0.3589	0.3873	0.4151	0.4406

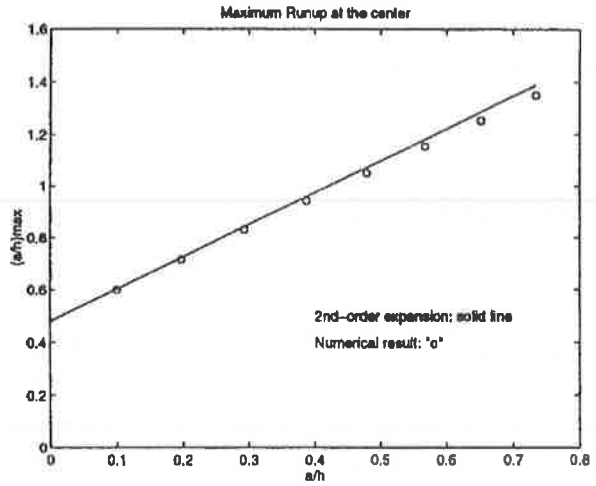

Fig. 9. Run-up at the place of the collision: (o) numerical; solid line: second-order expansion.

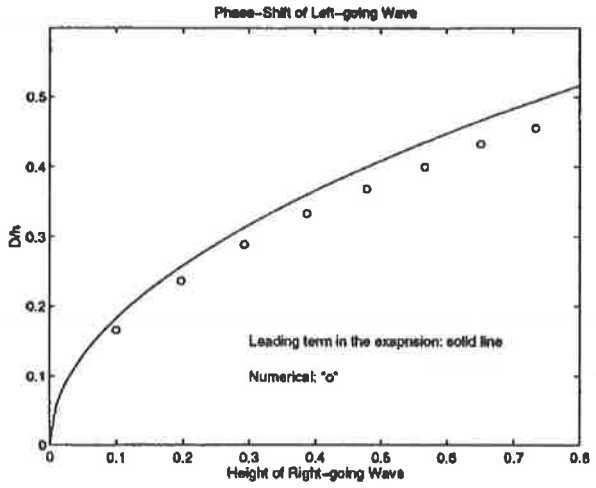

Fig. 10. Phase shift.

6. Summary

In this present paper, we investigated various aspects of a Boussinesq-type system of equations for the evolution of disturbances on the surface of water. For waves that do not vary significantly in the coordinate perpendicular to the primary direction of propagation, as with waves in a channel or long-crested waves on large bodies of water, we find the system studied here to be a good candidate for modeling long waves of small to moderate amplitude. In addition to admitting an appropriate theory of well-posedness for suitable initial-boundary-value problems, it is straightforward to construct accurate, efficient numerical schemes for the approximation of the system's solutions. We suggested a numerical scheme which is fourth-order accurate in both its spatial and its temporal approximation, which is unconditionally stable and which features good accuracy for work expended. The scheme is based on a pair of integral equations equivalent to the system of differential equations that comprise the Boussinesq system. Because of this formulation, it is comparatively easy to impose boundary conditions without disturbing either the order of accuracy or the convergence and stability properties.

Our study also featured preliminary comparisons of the model's predictions made via a computer code constructed on the basis of the numerical scheme analyzed in Section 3, with theoretical results derived from the Euler equations and with experimental results. In the numerical experiments connected with the head-on collision of solitary waves, we find our results to correspond well with facts about such interactions derived from the full Euler equations. There are quantitative differences between what is predicted on the basis of our model and experimental results, however. Earlier works based on unidirectional models for water-wave propagation indicate that it is likely that the absence of an accurate rendering of dissipative effects accounts for a good deal of the discrepancy.

A further study is planned along the lines set forth in [4] for unidirectional propagation, in which dissipation is incorporated and detailed comparisons are made with dynamically recorded wave data.

Acknowledgements

This work was supported in party by NSF grants DMS-9410188 and DMS-9622858 and by a Keck Foundation grant. JLB gratefully acknowledges CNRS support at the Centre de Mathématiques et de Leurs Applications, Ecole Normal Superieure de Cachan.

References

[1] C.J. Amick, J.F. Toland, On solitary waves of finite amplitude, Arch. Rational Mech. Anal. 76 (1981) 9–95.
[2] T.B. Benjamin, J.L. Bona, J.J. Mahony, Model equations for long waves in nonlinear dispersive systems, Phil. Trans. Roy. Soc. London Ser. A 272 (1972) 47–78.
[3] J.L. Bona, V.A. Dougalis, An initial- and boundary-value problem for a model equation for propagation of long waves, J. Math. Anal. Appl. 75 (1980) 503–522.
[4] J.L. Bona, W.G. Pritchard, L.R. Scott, An evaluation of a model equation for water waves, Phil. Trans. Roy. Soc. London Ser. A 302 (1981) 457–510
[5] J.L. Bona, W.G. Pritchard, L.R. Scott, Numerical schemes for a model for nonlinear dispersive waves, J. Comp. Phys. 60 (1985) 167–186.
[6] J.L. Bona, J.-C. Saut, J.F. Toland, Boussinesq equations for small-amplitude long wavelength water waves, preprint, 1997.
[7] J.L. Bona, R. Smith, A model for the two-way propagation of water waves in a channel, Math. Proc. Cambridge Phil. Soc. 79 (1976) 167–182.
[8] J. Boussinesq, Théorie de l'intumescence liquide appelée onde solitaire ou de translation se propageant dans un canal rectangulaire, Comptes Rendus de l'Acadmie de Sciences 72 (1871) 755–759.
[9] J.G.B. Byatt-Smith, An integral equation for unsteady surface waves and a comment on the Boussinesq equation, J. Fluid Mech. 49 (1971) 625–633.

[10] J.G.B. Byatt-Smith, The reflection of a solitary wave by a vertical wall, J. Fluid Mech. 197 (1988) 503–521.
[11] F.E. Camfield, R.L. Street, Shoaling of solitary waves of small amplitude, ASCE J., Waterwaves and Harbors Division 95 (1969) 1–22.
[12] R.K.-C. Chan, R.L. Street, A computer study of finite-amplitude water waves, J. Comput. Phys. 6 (1970) 68–94.
[13] M. Chen, Explicit tavelling-wave solutions of model systems describing bidirectional water waves, 1997, in preparation.
[14] M. Chen, J.L. Bona, Study of higher-order Boussinesq systems for water waves, preprint, 1995.
[15] W. Craig, An existence theory for water waves, and Boussinesq and Korteweg–de Vries scaling limits, Comm. Partial Diff. Eqs. 10 (1985) 787–1003.
[16] P. Davis, P. Rabinowitz, Methods of Numerical Integration, Academic Press, New York, 1984.
[17] J.D. Fenton, A ninth-order solution for the solitary wave, J. Fluid Mech. 53 (1972) 257–271.
[18] J.D. Fenton, M.M. Rienecker, A Fourier method for solving non-linear water-wave problems: application to Solitary Wave Interaction, J. Fluid Mech. 118 (1982) 411–443.
[19] E. Isaacson, H.B. Keller, Analysis of Numerical Methods, Wiley, New York, 1966.
[20] T. Maxworthy, Experiments on collision between solitary waves, J. Fluid Mech. 76 (1976) 177–185.
[21] J.W. Miles, Obliquely interacting solitary waves, J. Fluid Mech. 79 (1977) 157–159.
[22] M. Oikawa, N. Yajima, Interaction of solitary waves; a perturbation approach to non-linear systems, J. Phys. Soc. Japan 34 (1973) 1093–1099.
[23] D.P. Renouard, F.J. Seabra Santos, A.M. Temperville, Experimental study of the generation, damping, and reflexion of a solitary wave, Dynamics of Atmospheres and Oceans 9 (1985) 341–358.
[24] J. Scott Russell, Report on waves, Report on the Fourteenth Meeting of the British Association for the Advancement of Science, 1844.
[25] C.H. Su, R.M. Mirie, On head-on collisions between two solitary waves, J. Fluid Mech. 98 (1980) 509–525.
[26] C.J. Tang, V.C. Patel, L. Landweber, Viscous effects on propagation and reflection of solitary waves in shallow channels, J. Comput. Phys. 88 (1990) 86–113.
[27] G.B. Whitham, Linear and Nonlinear Waves, Wiley, New York, 1974.